Dynamics of $\eta \to \pi^+ \pi^- \pi^0$

F. Ambrosino, T. Capussela, F. Perfetto
Dipartimento di Scienze Fisiche Università degli Studi di Napoli "Federico II"
e Sezione INFN, Napoli

Abstract

A study of the dynamics of the decay $\eta \to \pi^+\pi^-\pi^0$ using the statistics of $\simeq 450\,\mathrm{pb}^{-1}$ collected in years 2000 to 2002 is presented. From a fit to the Dalitz plot density distribution we obtain a precise measurement of the slope parameters that can improve the knowledge of the decay amplitude and allow the test of theoretical predictions at the level of precision needed to extract the quark mass ratio (m_s^2 - $\hat{m}^2$)/(m_d^2 - m_u^2) from the decay rate ($\hat{m}$ is the u, d average mass).

1 Introduction

The decay of the isoscalar η into three pions occurs primarily through strong isospin violation and thus could be sensitive to the up-down quark mass difference. The electromagnetic corrections to the decay are small (Sutherland 's theorem [1]) and modify neither rate nor the Dalitz plot distributions noticeably [2].
To lowest order in the chiral expansion the decay amplitude is given by [3]:

$$A(s,t,u) = \frac{1}{Q^2}\frac{m_K^2}{m_\pi^2}\left(m_\pi^2 - m_K^2\right)\frac{M(s,t,u)}{3\sqrt{3}F_0^2} \tag{1}$$

where

$$Q^2 \equiv \frac{m_s^2 - \hat{m}^2}{m_d^2 - m_u^2} \tag{2}$$

is a combination of quark masses and $\hat{m} = \frac{1}{2}(m_u + m_d)$ is the average u, d quark mass, $F_0 = 92.4$ MeV is the pion decay constant and $M(s,t,u)$ contains all the dependance of the amplitude on the Mandelstam invariants. Since the decay rate is proportional to Q^{-4},

$$\Gamma\left(\eta \to \pi^+\pi^-\pi^0\right) \propto |A|^2 \propto Q^{-4} \tag{3}$$

the transition $\eta \to 3\pi$ represents in principle an extremely sensitive probe, allowing a determination of Q. Of course, in order to extract the quark mass ratio from the decay width, one has to have an accurate description of $M(s,t,u)$.
At lowest order

$$M(s,t,u) = \frac{3s - 4m_\pi^2}{m_\eta^2 - m_\pi^2}. \tag{4}$$

a well known result, obtained using Current Algebra. To cross-check the validity of the theoretical description one can use the Dashen theorem [1] [4] to determine Q:

$$Q^2_{Dashen} = \frac{m_K^2}{m_\pi^2} \frac{m_K^2 - m_\pi^2}{m_{K^0}^2 - m_{K^+}^2 + m_{\pi^+}^2 - m_{\pi^0}^2} \tag{5}$$

and integrate $M(s,t,u)$ over the phase space to predict the decay width, which has been determined quite accurately. Numerically, $Q_{Dashen} = 24.1$ and the corresponding prediction for the decay rate using LO result eq.(4) is:

$$\Gamma^{theo}\left(\eta \to \pi^+\pi^-\pi^0\right) = 88 \text{ eV} \tag{6}$$

in strong contraddition to the experimental result[18]:

$$\Gamma^{exp}\left(\eta \to \pi^+\pi^-\pi^0\right) = 295 \pm 16 \text{ eV}. \tag{7}$$

A one-loop calculation within conventional chiral perturbation theory (χPT) [6], improves the result considerably

$$\Gamma^{theo}\left(\eta \to \pi^+\pi^-\pi^0\right) \simeq 167 \pm 50 \text{ eV}. \tag{8}$$

but still fails in being in agreement with phenomenological value.
Further corrections discussed in the literature [5] may slightly increase the theoretical result, but cannot account for the large discrepancy to the data. On the other hand, a significant violation of the Dashen theorem (a different value for Q) could easily account for the discrepancy, but can be demonstrated only after comparison of the theoretical prediction for $M(s,t,u)$ with the experimental findings for the dynamics of the decay. The above discussion motivates a precise measurement of the $\eta \to 3\pi$ dynamics via the study of the Dalitz plot.
In the following, after a brief review on experimental results on the Dalitz plot parameters, the analysis is described and the results are presented.

2 Brief review of experimental results on the Dalitz plot parameters

The dynamics of the $\eta \to \pi^+\pi^-\pi^0$ decay can be studied with the usual method of the Dalitz plot analysis. It is based on the fact that in the centre of mass system, a 3-body decay has 2 free parameters. The choice of this pair of variables can be done in several way. Conventionally one uses the kinetic energies of the particles T_+, T_- and T_0 in the η rest frame and defines:

$$X = \sqrt{3}\frac{T_+ - T_-}{Q_\eta} = \frac{\sqrt{3}}{2M_\eta Q_\eta}(u - t) \tag{9}$$

$$Y = \frac{3T_0}{Q_\eta} - 1 = \frac{3}{2M_\eta Q_\eta}\left[((m_\eta - m_{\pi^0})^2 - s\right] - 1 \tag{10}$$

$$Q_\eta = m_\eta - 2m_{\pi^+} - m_{\pi^0} \tag{11}$$

where X and Y are respectively define in the range $[-1,1]$ and $[-1, 0.895]$.
The amplitude decay $A(X,Y)$ is then expanded about the center of Dalitz-plot as:

$$|A(X,Y)|^2 \simeq 1 + aY + bY^2 + cX^2. \tag{12}$$

[1] The Dashen theorem states that in the chiral limit the electromagnetic part of the kaon and pion electromagnetic mass shifts are the same: $\left(m^2_{\pi^+} - m^2_{\pi^0}\right)_{em} = \left(m^2_{K_+} - m^2_{K^0}\right)_{em}$

The amplitude is symmetric in X, therefore no odd power of X occurs in $|A(X,Y)|^2$.
The theoretical and experimental measurements of the slopes parameters are listed in Tab.1 and 2.
Unfortunately both experimental and theoretical scenario are not clear. All the measurements are

	a	b	c
tree	-1.00	0.25	0.00
one-loop [6]	-1.33	0.42	0.08
dispersive [7]	-1.16	0.26	0.10
tree dispersive [5]	-1.10	0.31	0.001
absolute dispersive [5]	-1.21	0.33	0.04

Table 1: Theoretical results for the slope parameters of the various approximations.

	N_η	a	b	c
Layter [8]	80884	-1.08 ± 0.14	0.034 ± 0.027	0.046 ± 0.031
Gormley [9]	30000	-1.17 ± 0.02	0.21 ± 0.03	0.06 ± 0.04
Crystal Barrel [10]	1077	-0.94 ± 0.15	0.11 ± 0.27	
Crystal Barrel [11]	3230	-1.22 ± 0.07	0.22 ± 0.11	0.06 fixed

Table 2: Experimental results for the slope parameters.

characterized by quite large uncertainties, moreover the parameter values are difficult to compare because making assumptions on the values of the quadratic slope significantly alters the fitted results of the others. A new measurement of the spectral shape, with higher statistics, would allow the determination of the existing disagreement between experimental findings and the theoretical predictions based on χPT are caused by an inaccurate value for the $d-u$ quark mass difference or to the importance of higher order final state interaction effects.

3 Selection of $\eta \to \pi^+\pi^-\pi^0$ decays

At KLOE the η meson is produced in the process $\phi \to \eta\gamma$, so to study the dynamic of $\eta \to \pi^+\pi^-\pi^0$ the final state is $\pi^+\pi^-\gamma\gamma\gamma$ which corresponds to a BR value of:

$$BR_{TOT} = BR\left(\phi \to \eta\gamma\right) \times BR\left(\eta \to \pi^+\pi^-\pi^0\right) \times BR\left(\pi^0 \to \gamma\gamma\right) = 2.9 \cdot 10^{-3}. \tag{13}$$

There is no combinatorial problem in the photon pairing because this decay chain is characterized by a monochromatic recoil photon, $E_{\gamma_{rec}} \sim 363$ MeV, whose energy is higher than the one of the photons coming from π^0 decay (see fig.1).

3.1 Selection cuts

The events selection is performed through the following step:

1. Events are selected starting from the RAD stream with charged particles [12].

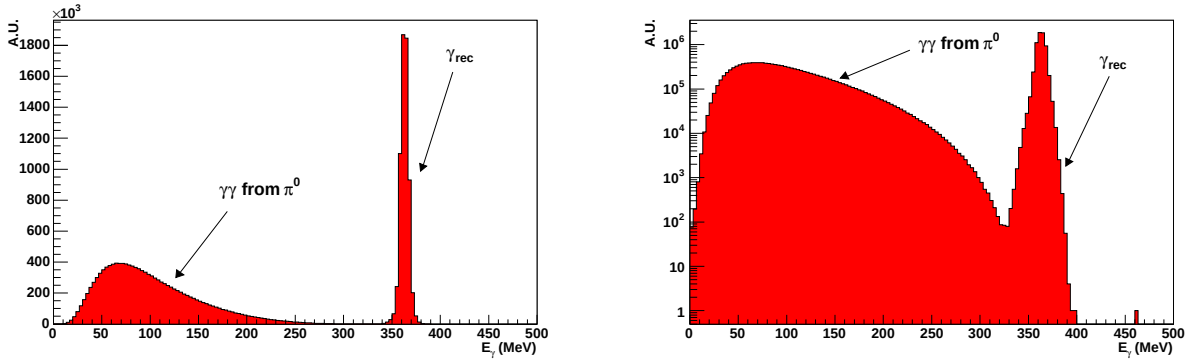

Figure 1: MonteCarlo photon energy spectrum. Left: linear scale; Right: log scale.

2. One charged vertex is required inside the cylindrical region $r < 4$ cm, $|z| < 8$ cm and 3 prompt neutral clusters [2] (*pnc*) with $\theta_\gamma > 21°$ and $E_\gamma > 10$ MeV. To reduce the problem of cluster splitting a cut on the opening angle between each couple of photons is done $\theta_{i,j} > 18°$.

3. E_{prompt} [3] $< 800\,\text{MeV}$. This cut is already present in the PPFILT EVCL algorithm. We repeat it at the analysis level to remove few events selected in the RAD stream by algorithms other than PPFILT.

4. A constrained kinematic fit is performed requiring 4-momentum conservation and the speed of light for each photon, without imposing mass constraint both on η and π^0 .
   A cut on the χ^2 probability is done, $\mathcal{P}(\chi^2) > 1\%$.
   The effect of this fit on the event reconstruction is to improve significantly the resolution on photon energies and invariant masses. We note in passing that, due mainly to the improvements in MC simulations, the distribution of the χ^2 variable of the fit (fig.2) shows a better agreement data - MC than it was in the past [15].

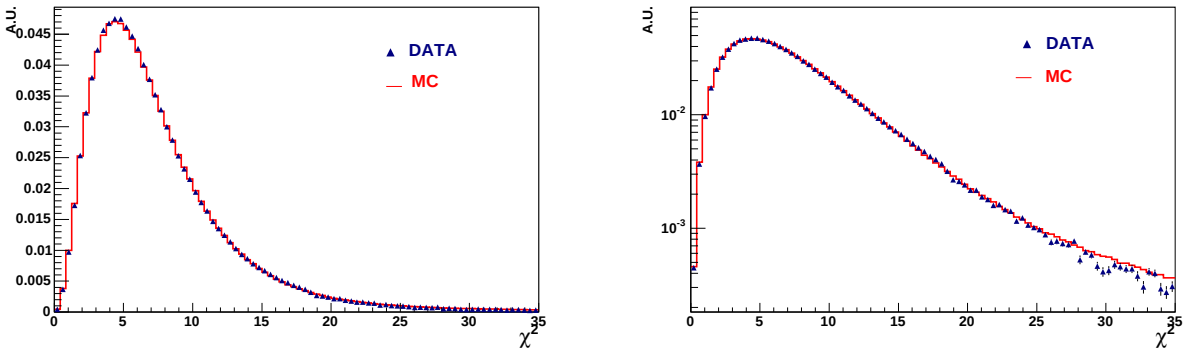

Figure 2: χ^2 distribution. Left: linear scale; Right: log scale.

[2] A *pnc* is defined as a cluster in the EmC with no associated track coming from the Drift Chamber (DC) and $|(t - \frac{r}{c})| < 5\sigma_t$ where t is the arrival time on the EmC, r is the distance of the cluster from the IP and c is the speed of light and $\sigma_t = 54\,\text{ps}/\sqrt{E(\text{GeV})} \oplus 147\,\text{ps}$[13].

[3] For every event the prompt energy is defined as the sum of the energies of all the *pnc*

5. Finally we require:

   - $320\,\text{MeV} < E_{\gamma rec} < 400\,\text{MeV}$ (reduces the residual background from $\phi \to K_S\,K_L$ events).
   - $E_{\pi^+} + E_{\pi^-} < 550\,\text{MeV}$ (reduces the residual background from $\phi \to \pi^+\pi^-\pi^0$events).
   - $M_{\gamma\gamma} \in [110, 160]$ [4] (reduces the residual background from $\phi \to \eta\gamma$ events, with $\eta \to \pi^+\pi^-\pi^0$ and $\pi^0 \to e^+e^-\gamma$; and from $\phi \to \eta\gamma$ events, with $\eta \to \pi^+\pi^-\gamma$).
     Fig.3 shows the comparison data MonteCarlo for the variable used in the cut, the observed discrepancy is due to the presence of background.

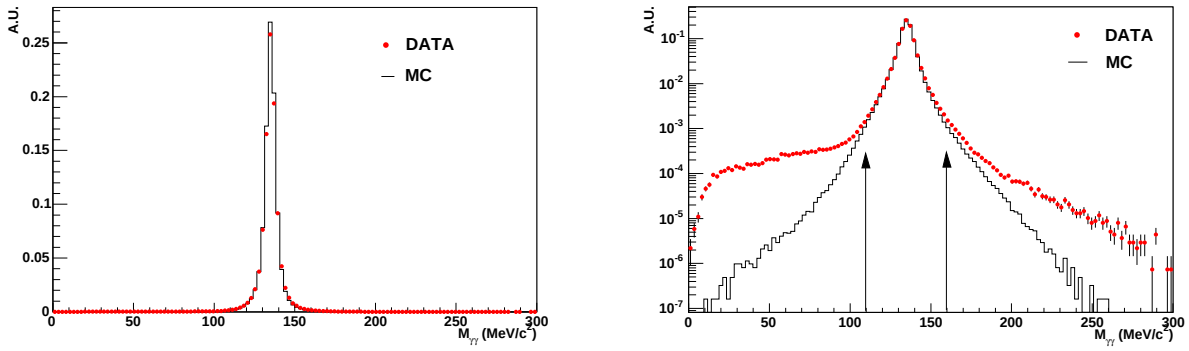

Figure 3: Data vs MonteCarlo comparison for the invariant mass of the two softest photons in $\pi^+\pi^-\gamma\gamma\gamma$ events. Left: linear scale; Right: log scale. The arrows show the cut applied. The histograms are normalized to the same area.

3.2 Selection efficiency

For the different steps of selection the relative efficiencies are estimated. In particular:

- The trigger efficiency evaluated by MonteCarlo is 99.9%, so the effect of trigger has been neglected. The good data - MC agreement for the trigger sector multiplicities is shown in fig.5.

- The effect of the event classification procedure (EVCL) and machine background filter (FILFO) is evaluated using a downscaled sample, minimum bias, with less stringent event classification cuts [16].
  The efficiency of minimum bias algorithm has been evaluated on a MonteCarlo sample, we find on events selected by the analysis

$$\varepsilon = (99.88 \pm 0.01)\% \tag{14}$$

  this means that the minimum bias events are a good sample to test the bias introduced by EVCL procedure. The selection procedure has been applied to this data sample without using the EVCL selection and the result has been compared to the selection procedure including EVCL applied on the same data set. A similar analysis has been done to check FILFO.
  While the FILFO algorithm is absolutely negligible, the EVCL procedure introduces an inefficiency of $\sim$ 1.5% on the selected events. In the following, the effect of this bias on the parameters

[4] $M_{\gamma\gamma}$ is the invariant mass of the two softest photons in $\pi^+\pi^-\gamma\gamma\gamma$ events.

measurement will be analysed.

No difference between data and MC on the overall efficiency is observed:

$$\varepsilon_{EVCL}^{data} = (98.53 \ \pm \ 0.07)\% \tag{15}$$

$$\varepsilon_{EVCL}^{MC} = (98.55 \ \pm \ 0.01)\%. \tag{16}$$

- The tracking and vertex efficiencies have been checked selecting $\phi \to \pi^+\pi^-\pi^0$ from raw data[17]: The DATA-MC ratio of efficiencies is flat all over the momentum spectrum, see fig4, thus introducing no bias in the Dalitz plot fit. We must stress that all the variables used in the fit are evaluated in the η rest frame, which is boosted with respect to the laboratory by about 363 MeV. This means that the content of each bin in momentum in the LAB frame is actually distributed all over the momentum range in the η cms used for the fit: any DATA-MC discrepancy in the LAB system is further diluted by this effect. The data-MonteCarlo ratio of the overall tracking and vertex efficiences is :

$$\frac{\left(\varepsilon_{TRK}^2 \varepsilon_{VTX}\right)_{DATA}}{\left(\varepsilon_{TRK}^2 \varepsilon_{VTX}\right)_{MC}} = 0.974 \ \pm \ 0.006. \tag{17}$$

After this cuts the overall selection efficiency is $\varepsilon = (33.6 \ \pm \ 0.2)\%$. [5]

[5]The MC efficiency has been corrected for the data/MC ratio of efficiencies for low energy photons (see section 8.2), and for data/MC ratio of the overall tracking and vertex efficiencies.

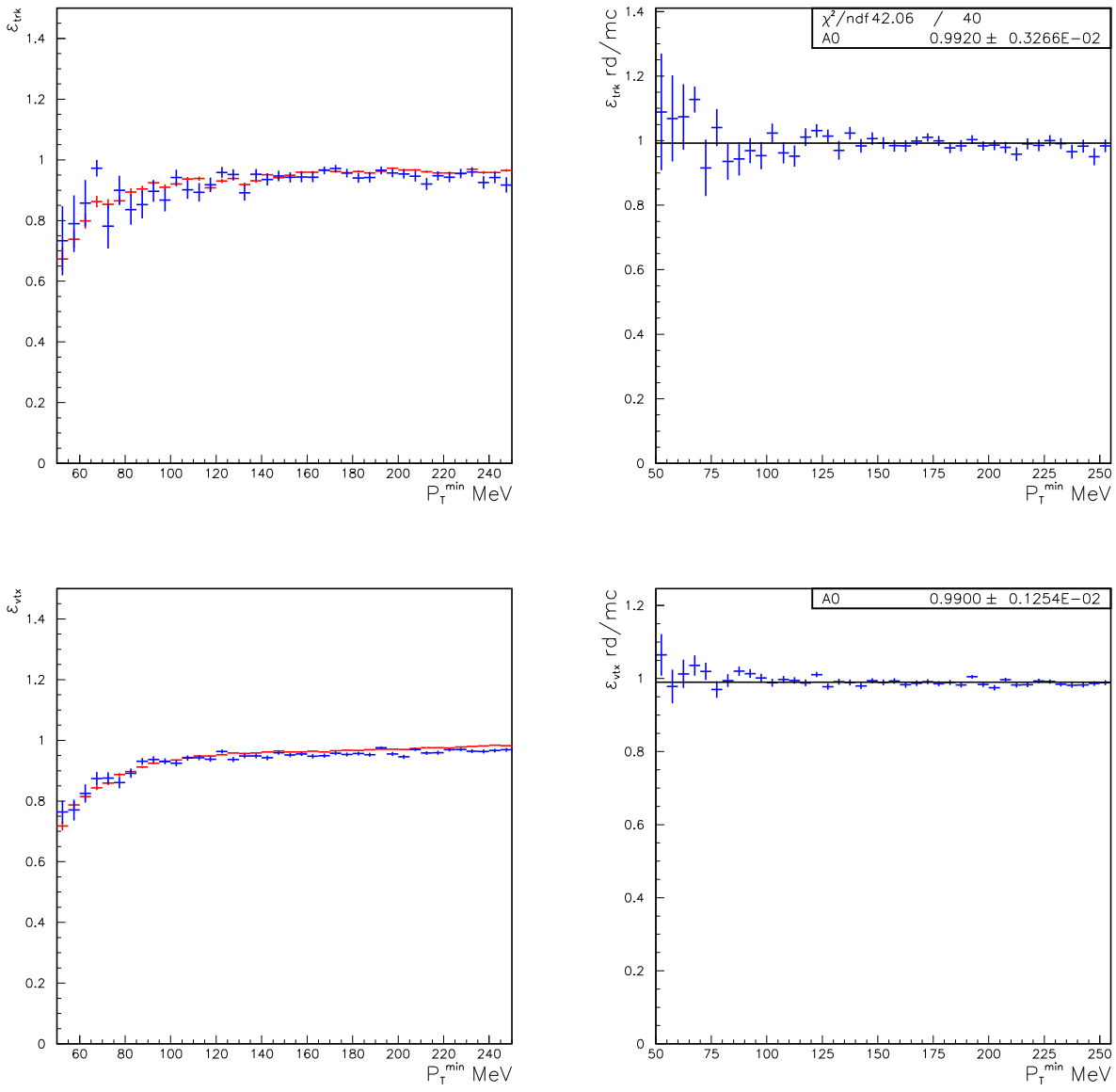

Figure 4: Left: Tracking (upper plot) and Vertex (lower plot) efficiency as function of minimum P_T of the two tracks. Right: Data (blue) MonteCarlo (red) ratio for the tracking (upper plot) and vertex (lower plot) efficiencies.

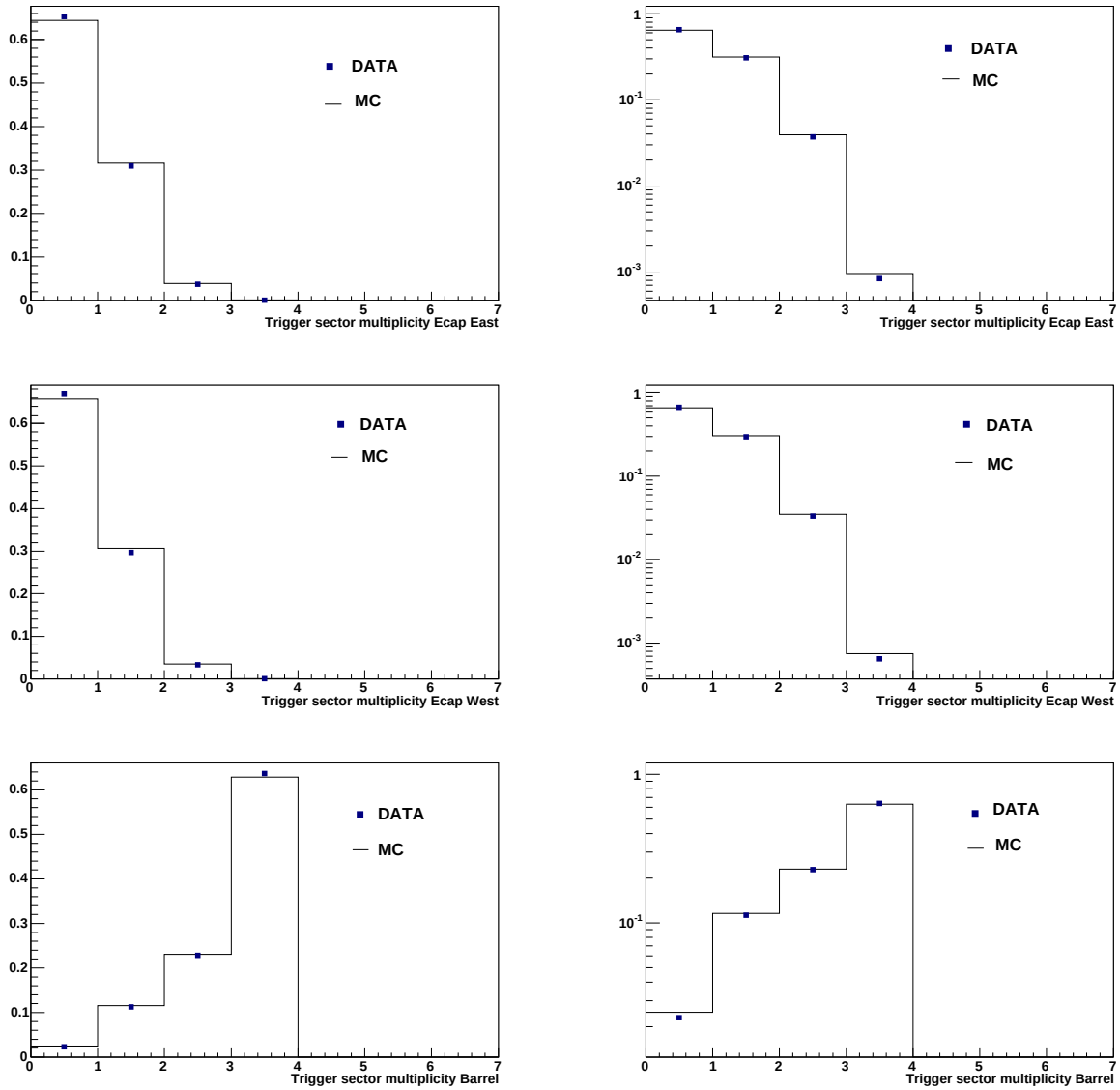

Figure 5: Trigger sector multiplicity. From top to bottom: endcap East, endcap West, barrel. Left: linear scale. Right: log scale.

4 Analysis on MC

4.1 Resolution and efficiency on Dalitz-plot variables

The Dalitz-plot variables are evaluated using the measured momenta of the pions boosted in to the η rest frame. In particular, the four-momenta of the pions are obtained: for $\pi^{\pm}$, from the track parameters (curvature, azimuthal-angle ϕ and cotg θ) and for π^0 , from the information about the photons generated in the π^0 decay (E, x, y, z, t for each photons).

The resolution on the Dalitz variables (X, Y) is shown in fig.6 where the differences between the recon-

structed values (X_{rec}, Y_{rec}) and the true values (X_{gen}, Y_{gen}) are plotted. A sum of 4 gaussians nicely fits

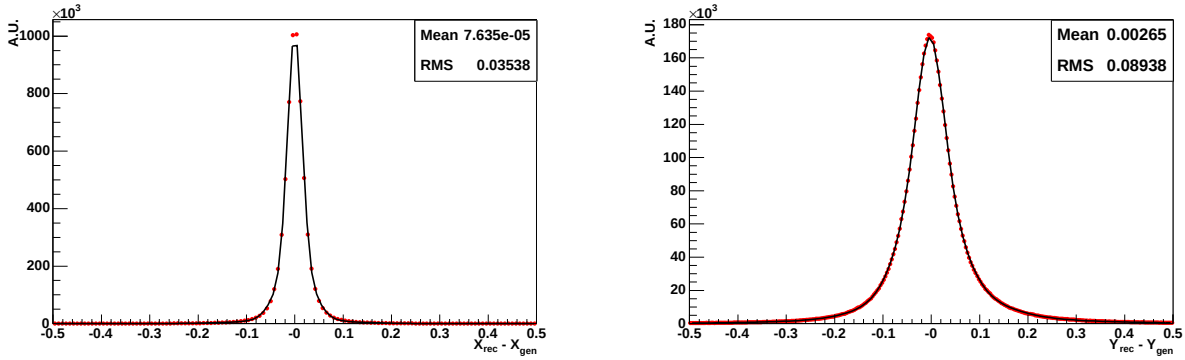

Figure 6: MonteCarlo distributions of resolutions: X (left) and Y (right). The curves are fitted to a sum of four gaussians.

each of the two distribution. The width of the "core" gaussian

$$\delta X = 0.020 \qquad\qquad \delta Y = 0.026 \tag{18}$$

gives an estimate of the resolution.
In order to improve the resolution on Y variable we note that a second way to compute Y is possible. In fact, we can obtain the kinetic energy of π^0 from the $\pi^+$and π^-energy:

$$T_0^{ch} = M_\eta - (E_{\pi^+} + E_{\pi^-}) - M_{\pi^0} \tag{19}$$

so we define:

$$Y_{ch} = \frac{3T_0^{ch}}{Q_\eta} - 1 \tag{20}$$

which is slightly better in resolution (see fig.7)

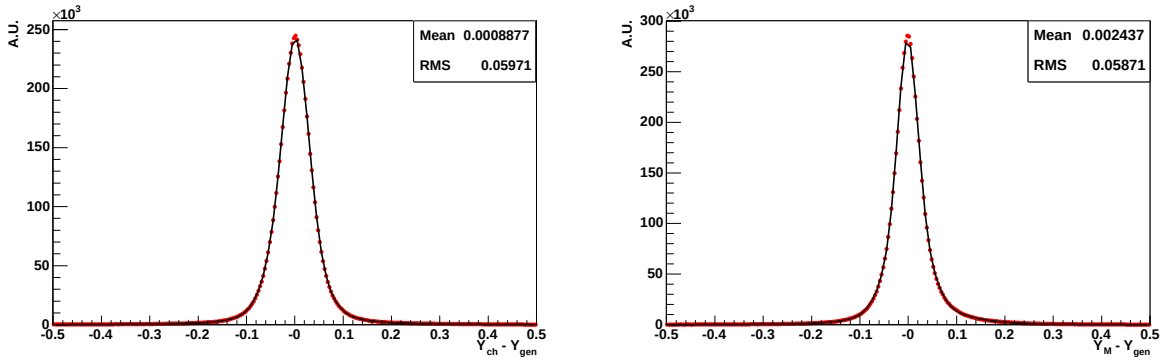

Figure 7: MonteCarlo distributions of resolutions: Y_{ch} (left) and Y_M (right). The curves are fitted to a sum of four gaussians.

$$\delta Y_{ch} = 0.025. \tag{21}$$

Finally, MonteCarlo studies demonstrate that the best evaluation of Y resolution is given using the average between the two variables:

$$Y_M = \frac{Y_{ch} + Y}{2}. \tag{22}$$

and the corresponding resolution, see fig.7, is:

$$\delta Y_M = 0.019 \tag{23}$$

No relevant improvement in the resolution values has been observed imposing the costraint on the invariant mass of π^0. In the following Y will denote the Y_M variable, while we will refer to the variable obtained using only the photon energies as Y_0.
Fig.8 shows the comparison data-MonteCarlo for the variable $Y_{ch} - Y_0$. Applying a double-Gaussian fit

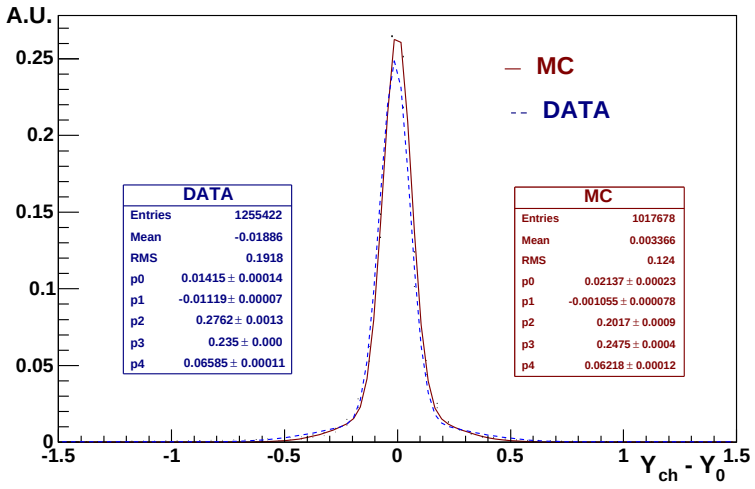

Figure 8: Data (continuos line) vs. MonteCarlo (shaded line) comparison for the variable $Y_{ch} - Y_0$. The curves are fitted to a sum of two gaussians with the same mean.

with the same mean value a data-MC shift of ~ 450 KeV on the $T_0^{ch} - T_0$ variable is estimated. This shift coming from a data-MonteCarlo discrepancy on the value of invariant mass of three pions system $\left(\pi^+\pi^-\pi^0\right)$. Indeed, the M_η value obtained fitting data (see fig.9) is different with respect to the MonteCarlo simulation, $M_\eta = 547.30$ MeV. The data-MonteCarlo discrepancy on the M_η value cannot be considered as an energy scale effect because for the same events no shift in the peak value of the $\gamma\gamma$ invariant mass is observed, see fig.10.

As expected, correcting the M_η value the data-MC shift on the $T_0^{ch} - T_0$ variable is reduced, we found a shift of ~ 10 KeV (fig.11). Finally, in order to improve the agreement between data and MonteCarlo we add to the selection procedure the cut:

$$|Y_{ch} - Y_0| < 0.5. \tag{24}$$

This cut is almost fully efficient on signal. The final selection efficiency is $\varepsilon = (33.4 \pm 0.2)\%$ [6].

[6]The MC efficiency has been corrected for the data/MC ratio of efficiencies for low energy photons (see section 8.2), and for data/MC ratio of the overall tracking and vertex efficiencies.

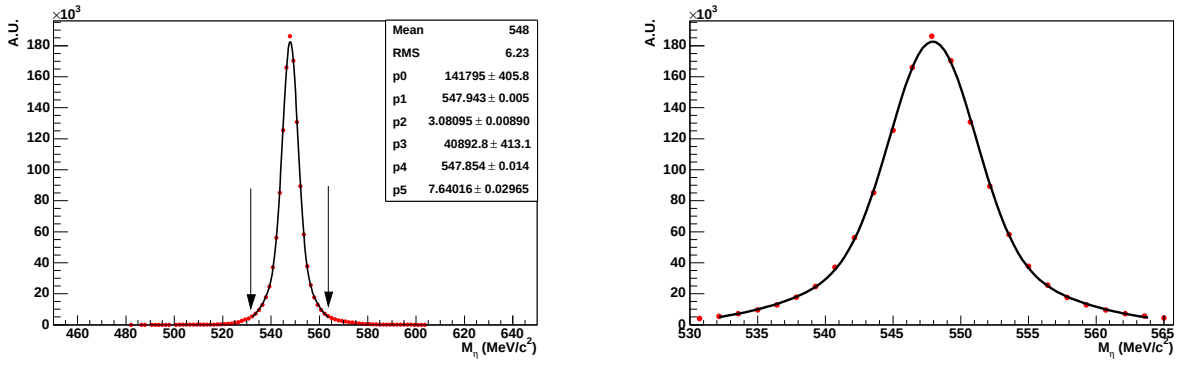

Figure 9: Distribution of the invariant mass of three pions system $\left(\pi^+\pi^-\pi^0\right)$ for the data sample used in this analysis. The arrows show the range of fit. Right: A zoom of the region of the fit. The M_η fitted value is in agreement with NA48 measurement [21]: $M_\eta = 547.843 \pm 0.030^{stat} \pm 0.041^{syst}$ MeV.

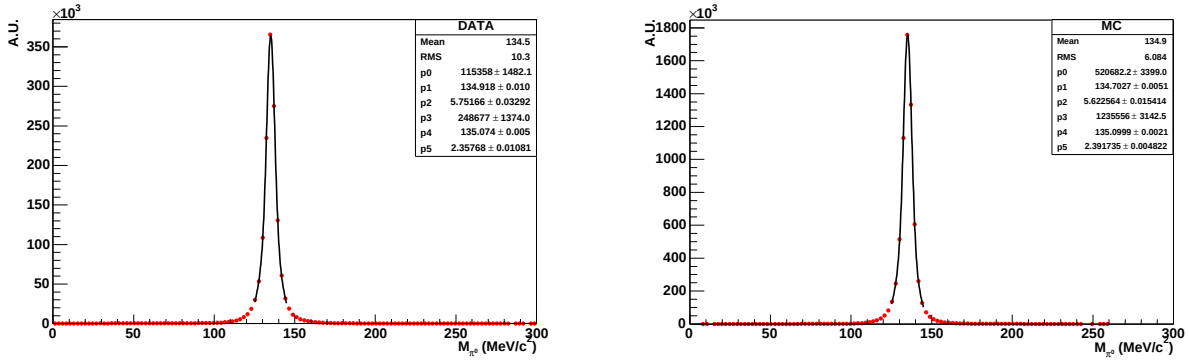

Figure 10: The invariant mass of the two softest photons in $\pi^+\pi^-\gamma\gamma\gamma$ events. Left: Data distribution. Right: MonteCarlo distribution.

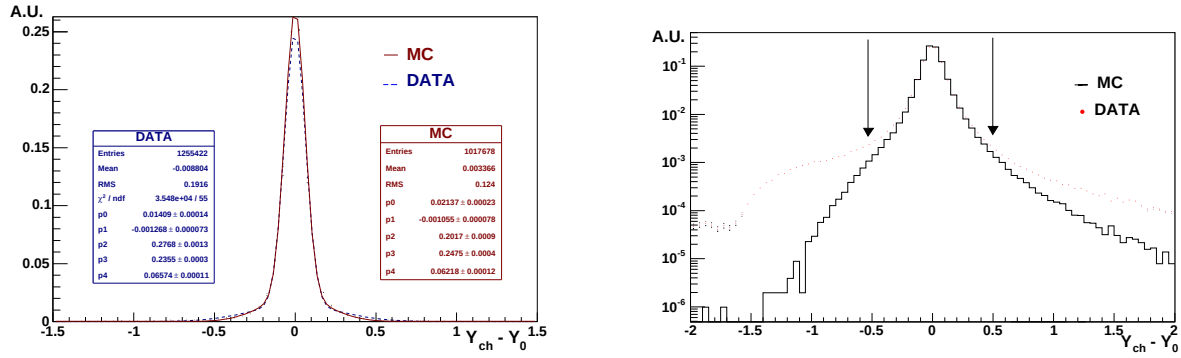

Figure 11: Data (continuos line) vs. MonteCarlo (shaded line) comparison for the variable $Y_{ch} - Y$ with the corrected value of M_η. Left: linear scale. Right: log scale. The arrows show the position of the cut eq: (24)

In the region characterized from $N_{binx} = N_{biny} \in [7, 20]$, or changing the linear dimensions of bins from $\Delta X = \Delta Y = 0.29$ to $\Delta X = \Delta Y = 0.10$, possible smearing effects are evaluated. These effects, being the linear dimensions of the bins used much larger than X and Y resolutions, cfr. eq.18, 23, are negligible. In particular, fig.12 shows the smearing matrix for X and Y variables in correspondence of a bin width choice:

$$\Delta X = \Delta Y = 0.13 \qquad or \qquad N_{binx} = N_{biny} = 16 \tag{25}$$

Along the straight lines:

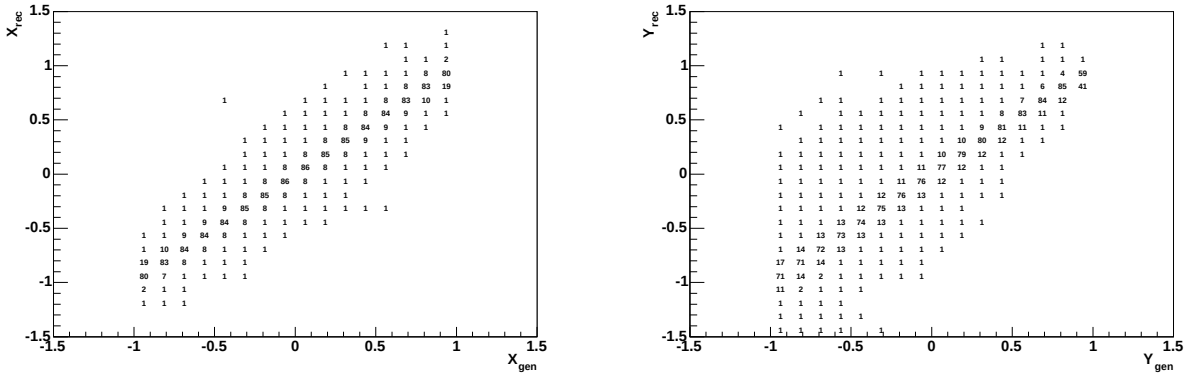

Figure 12: Smearing matrix distribution. Left: Xvariable; Right: Y variable.

$$X_{gen} = X_{rec} \qquad\qquad Y_{gen} = Y_{rec} \tag{26}$$

there are distributed respectively $\sim 84\%$ and $\sim 76\%$ of events while the rest of events crosses from a bin to the adjacent bins.

The efficiency as function of Dalitz plot point $\varepsilon(X, Y)$ is defined, for each (X, Y) bin, as the ratio between the number of events generated that are fully reconstructed and selected, or equivalently as the plot obtained with the bin-by-bin division

$$\varepsilon(X, Y) = \frac{N_{rec}(X, Y)}{N_{gen}(X, Y)} \tag{27}$$

where $N_{rec}(X, Y)$ is the reconstructed Dalitz distribution and $N_{gen}(X, Y)$ is the originarily MC generated Dalitz distribution. In fact it must be stressed that the definition of efficiency given above actually contains also the smearing effects integrated bin by bin over the MC histogram. This approach is equivalent to the use of the complete four-dimensional smearing matrix as long as the parameterization of the Dalitz plot shape used in the simulation is in good agreement with the real one. As described later in this note, we have used a low statistics data sample to obtain a first estimate of the parameters in order to better the MC description and then we have used the improved MC for determining the final result on the full statistics. The $\varepsilon(X, Y)$ (see fig.13) is almost flat in the central region of Dalitz-plot but presents few peaks on contour because in the corresponding bins the phase space is reduced and the contribution of nearby bins via the smearing effects is percentually larger. The projections of $\varepsilon(X, Y)$ on the X and Y axis are plotted in fig.14. While the efficiency appears to behave quite independently of X and preserve the symmetry property, it decreases in an approximately linear way as Y grows in the allowed interval. This can be explained through simple arguments. The X variable is proportional to a difference between

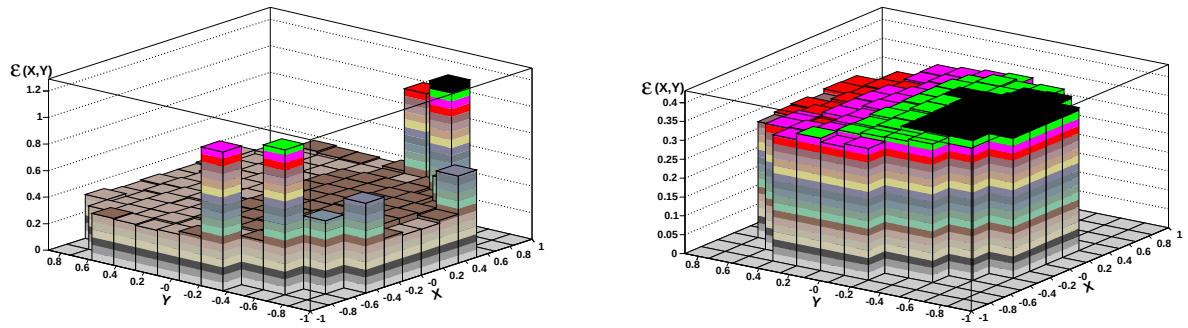

Figure 13: Efficiency as function of Dalitz-plot, before (left) and after (right) removing the bins intersected by Dalitz-plot contour.

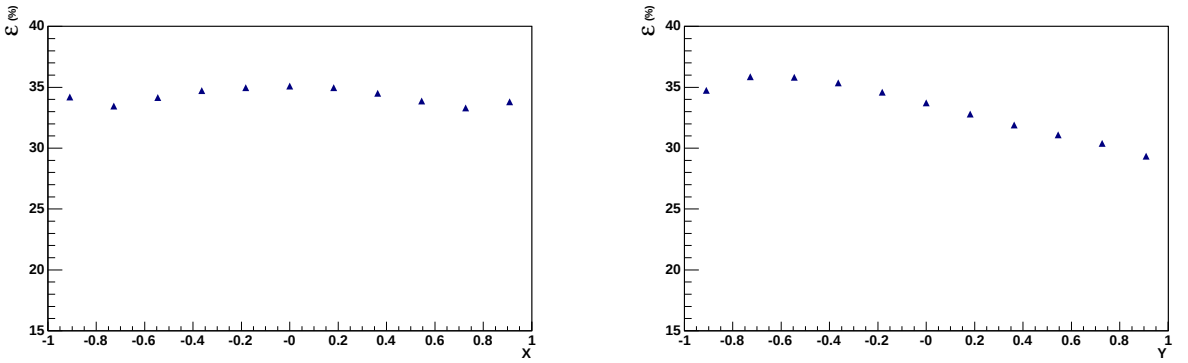

Figure 14: Left: Efficiency versus X. Right: Efficiency versus Y.

kinetic energies of $\pi^+$and π^-which behave similarly in the Drift Chamber and since we don't ask the track to cluster association we expect no asymmetry in the efficiency, apart from the one coming from possible residual magnetic field effects. In the average, a large value for Y means a low-momentum $\pi^\pm$ in the decay: this reduce the probability to correctly reconstruct the vertex and explains the slight drop in efficiency as Y rises.

5 Fit of Dalitz-plot procedure

The fit is done using a least squares approach. Let $|A(X,Y)|^2$ the theoretical function

$$|A(X,Y)|^2 \simeq N(1 + aY + bY^2 + cX + dX^2 + eXY). \tag{28}$$

and N_{ij} the number of events in the bidimensional bin (i,j), the χ^2 is:

$$\chi^2 = \sum_{i=1}^{N_{binx}} \sum_{j=1}^{N_{binx}} \left(\frac{N_{ij} - \varepsilon_{ij} \int_{x_i^{min}}^{x_i^{max}} \int_{y_i^{min}}^{y_i^{max}} |A(X,Y)|^2 dPh(X,Y)}{\sigma_{ij}} \right)^2 \tag{29}$$

where for each bin (i,j):

- ε_{ij} is the efficiency as function of Dalitz-plot,
- (x_i^{min}, x_i^{max}) and (y_j^{min}, y_j^{max}) are the boundary of bins in X and Y,
- σ_{ij} is the statistical error on the ratio $\frac{N_{ij}}{\varepsilon_{ij}}$, according to:

$$\sigma_{ij} = \frac{N_{ij}}{\varepsilon_{ij}} \sqrt{\frac{1}{N_{ij}} + \left(\frac{(\delta\varepsilon)_{ij}}{\varepsilon_{ij}} \right)^2} \tag{30}$$

- dPh(X,Y) is the phase space region.

All the bins are included in the fit apart from the bins crossed by the Dalitz-plot contour, in which fluctuations of efficiency are present.

6 Results of fit on MC

The procedure of fit described has been tested on MonteCarlo.
In order to exclude possible correlations that can affect the parameters evaluation the efficiency has been calculated on an independent sample. Initially we have analysed a sample of ~ 250000 pure $\phi \to \eta\gamma$ events, in which the phase space has been generated with these parameter values:

$$a = -1, \qquad b = c = d = e = 0. \tag{31}$$

Fig.15 shows how the fitted parameter values change with the number of degrees of freedom [7], *ndf*; at the same time the binning for the Dalitz-plot change from $N_{binx} = N_{biny} = 7$ to $N_{binx} = N_{biny} = 20$, in corrispondence the linear dimensions of bins change from $\Delta X = \Delta Y = 0.29$ to $\Delta X = \Delta Y = 0.10$. The choice of not increase further the binning is essentially driven by the resolution of the two variables X, Y (cfr. eq.18, 23): smearing effects can negatively affect the agreement between the data and the theoretical function.
As can be observed, the fitting procedure allows to find correctly the MonteCarlo input parameters (in fig.15 pointed out with the straight line) and moreover the measurements are almost *ndf* independent, to be precise binning independent.
Some parameters are strongly correlated , table 3 gives the correlation coefficients between the parameters. In particular b and d are anticorrelated with a, on the other hand c and e are less correlated to the other parameters. Thus we expect that fixing to zero the value of c and e the other ones will not change. In fact, see fig.16, considerable variations are not present.

[7] *ndf* is the difference between the number of effective bins fitted, removing the bins crossed by Dalitz-plot contour, and parameters measured: $ndf = N_{bin}^{eff} - P$.

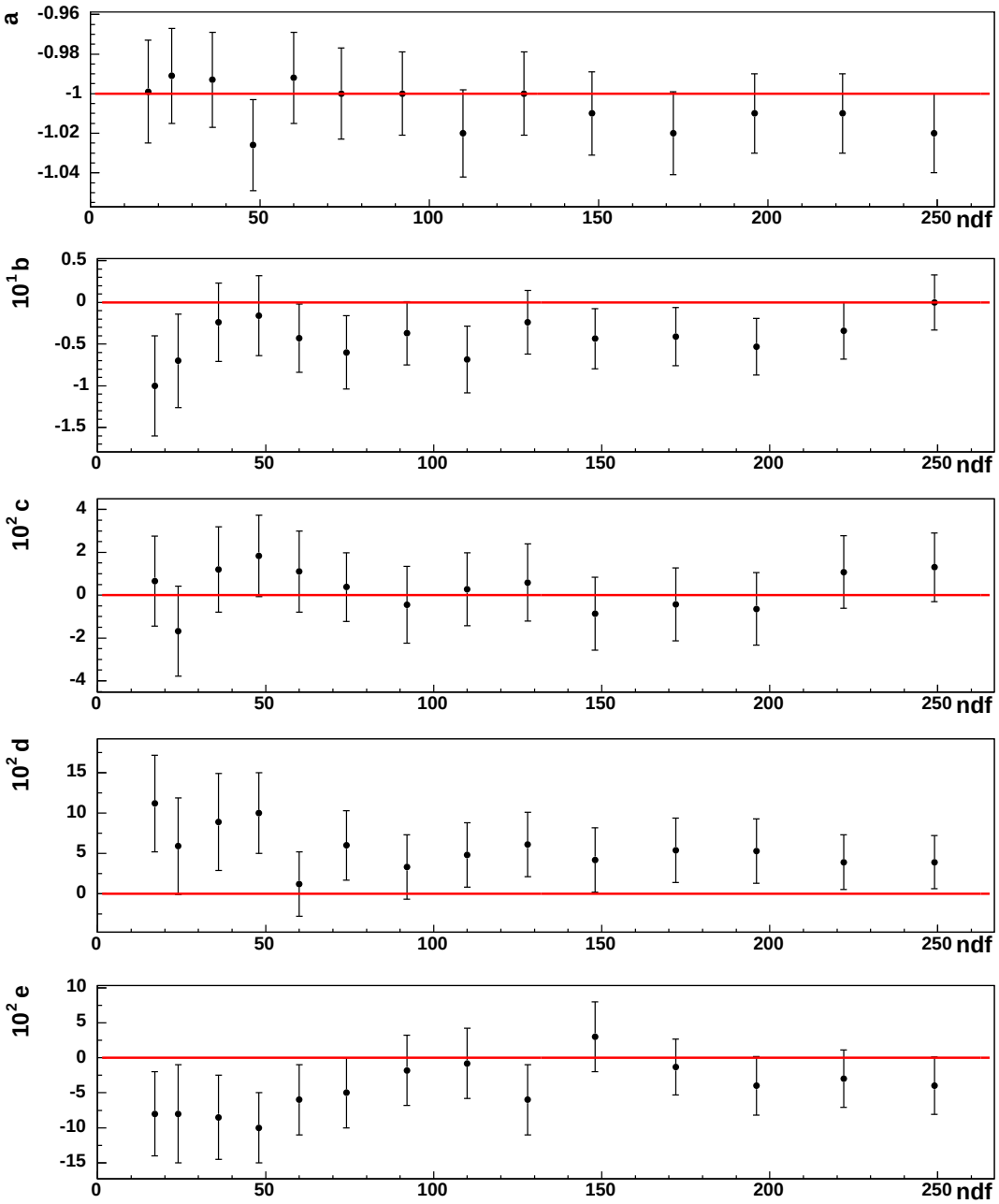

Figure 15: Results of the Dalitz-plot fit on first MC sample for different *ndf*. The results refer to a parametrization for the decay amplitude $|A(X,Y)|^2 \simeq 1 + aY + bY^2 + cX + dX^2 + eXY$. The MonteCarlo input parameters are pointed out with the straight line.

	a	b	c	d	e
a	1	-0.723	0.011	-0.442	-0.018
b		1	-0.056	0.311	0.053
c			1	0.052	-0.389
d				1	-0.065
e					1

Table 3: Correlation matrix from the Dalitz-plot fit on first MC sample.

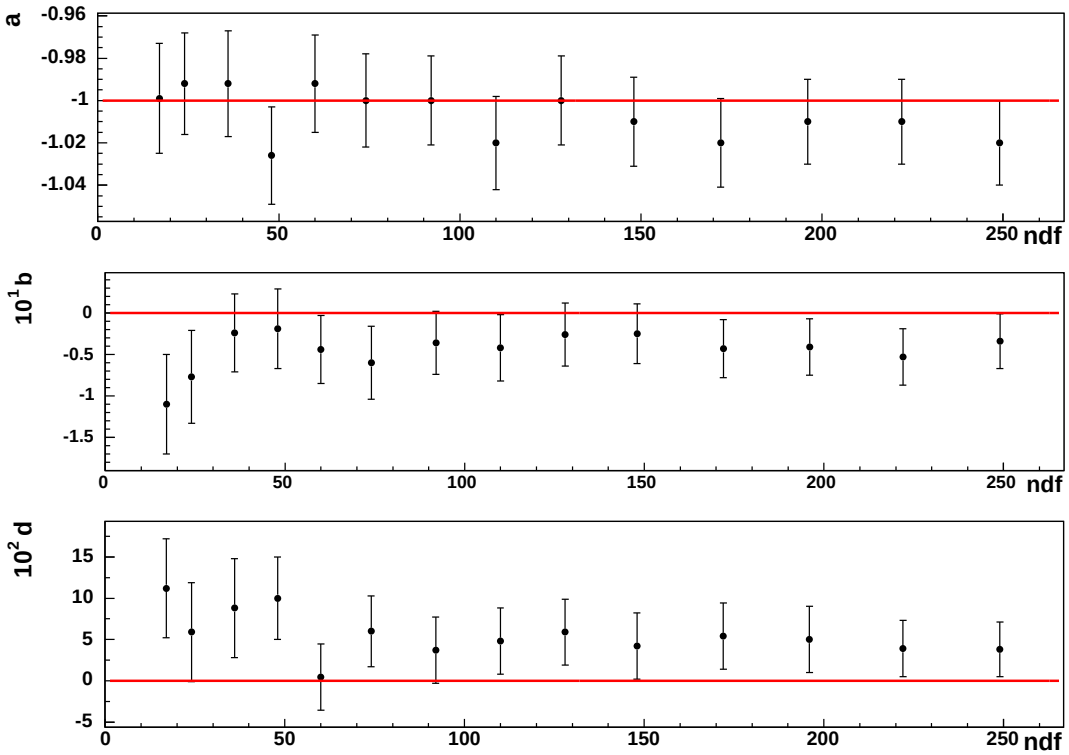

Figure 16: Results of the Dalitz-plot fit on first MC sample for different *ndf*. The results refer to a parametrization for the decay amplitude $|A(X,Y)|^2 \simeq 1 + aY + bY^2 + dX^2$. The fit is performed by setting to zero the parameter values c and e. The MonteCarlo input parameters are pointed out with the straight line.

7 Analysis on data

In order to give a precise measurement of the slope parameters the statistics, $\int Ldt = 451\,\mathrm{pb}^{-1}$, collected in 2000 to 2002 data taking is analysed.
The total expected number of $\eta \to \pi^+\pi^-\gamma\gamma\gamma$ events has been estimated using the visible cross section at ϕ peak [19], and the MC efficiency corrected for the data/MC ratio of efficiencies for low energy photons, and for the data/MC ratio of tracking and vertex efficiencies.

$$\sigma(\eta\gamma)_{visible-peak} = (40.2 \pm 1)\ \mathrm{nb} \tag{32}$$

$$N_{exp} = 1.35 \pm 0.04 \quad \mathrm{Mevts} \tag{33}$$

Whereas, the number of events in the Dalitz-plot, see fig.17, is:

$$N_{found} = 1.337 \pm 0.001 \quad \mathrm{Mevts} \tag{34}$$

We notice a difference at the level of 1.2%, and the two numbers are compatible within errors. Before analyzing the whole statistics, the procedure of fit has been applied on a data sample corresponding to $\int Ldt \sim 100\,\mathrm{pb}^{-1}$ collected in 2000 and 2001.

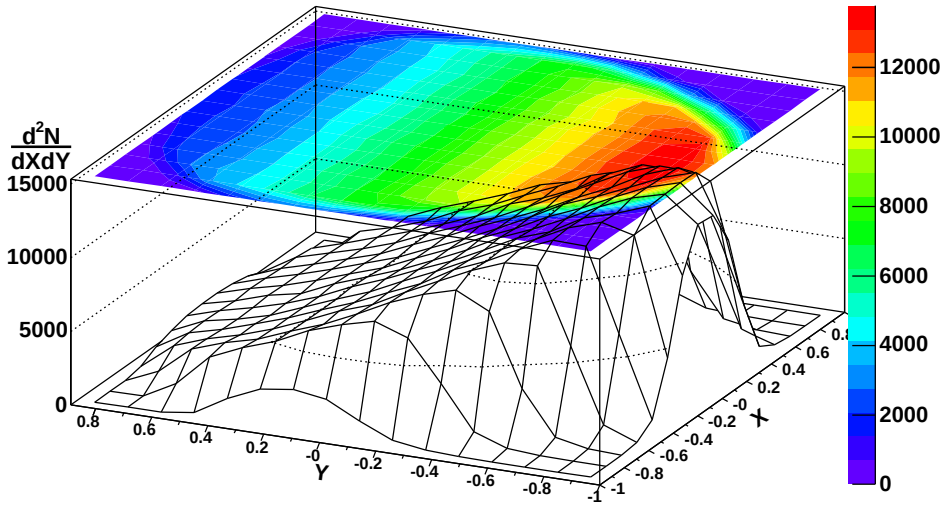

Figure 17: Dalitz-plot distribution observed on whole data sample. The plot contains 1.34 millions of events in 256 bins.

7.1 Results of fit on $2000 - 2001$ statistics

As made for the MonteCarlo, we have estimated the parameter values for different *ndf*, see fig.18.

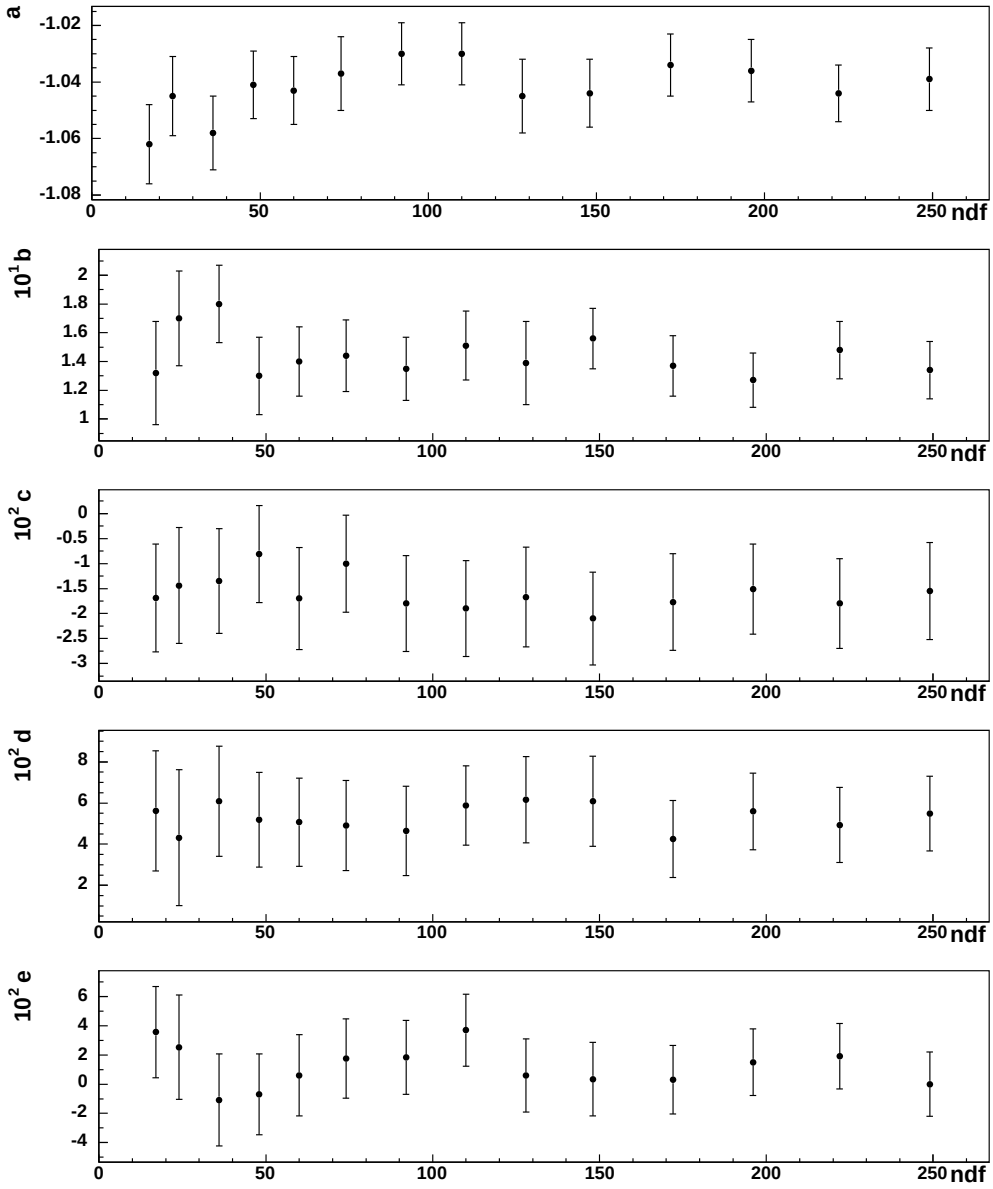

Figure 18: Results of the Dalitz-plot fit for different values of *ndf*. The results refer to a parametrization for the decay amplitude $|A(X,Y)|^2 \simeq 1 + aY + bY^2 + cX + dX^2 + eXY$.

After an initial instability essentially due to the low *ndf* available for the fit, the measures catch up a plateau region in which they are almost binning independent.
In correspondence of $N_{bin}^{eff} = 80$ (or for linear dimensions of bins equal to $\Delta X = \Delta Y = 0.17$), where we found the better χ^2 probability, we give the final evaluation of the slope parameters, see table 4. The quoted uncertainties on the parameters are those coming from the fit. The parameter values obtained fixing to zero the value of c and e have been inserted in the generator of the new MonteCarlo production used in the rest of this analysis, this allowed us to improve our simulation of the decay, with a more accurate determination of efficiencies within each bin. We have checked our ability to reproduce the values inserted into the new improved MonteCarlo simulation. The results are shown in fig. 19. We compare the values obtained in output from the fit with the ones used as input for the MonteCarlo production, and build a χ^2 variable, including the full covariance matrix as estimated by the fit. We get good agreement for each binning choice. In particular e.g. for the binning $N_{eff}^{bin} = 154$, which later we will show being the "best binning choice" on data, one finds a $\chi^2/\mathrm{dof} = 3.1/5$ with a χ^2 probability of 68% : this gives us confidence that our fitting procedure does not introduce a bias in the estimation of parameters.

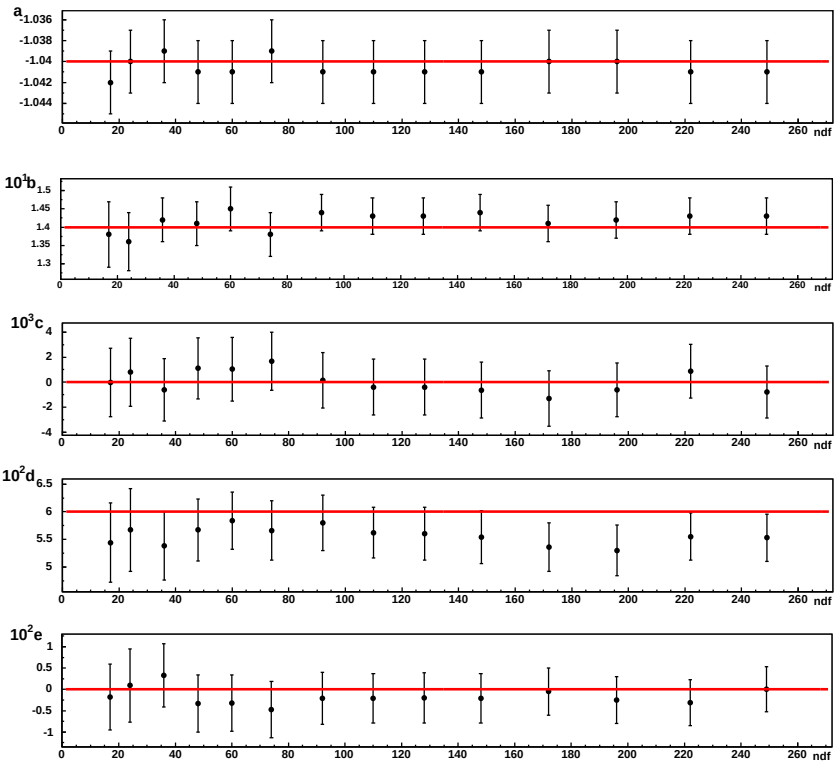

Figure 19: Results of the Dalitz-plot fit on the Monte Carlo improved simulation for different values of *ndf*. The results refer to a parametrization for the decay amplitude $|A(X,Y)|^2 \simeq 1 + aY + bY^2 + cX + dX^2 + eXY$. The horizontal lines show the values used as input for the simulation.

ndf	P_{χ^2}	a	b	c	d	e
74	65%	-1.04±0.01	0.14±0.03	-0.001±0.002	0.05±0.02	-0.02±0.03
76	68%	-1.04±0.01	0.14±0.03		0.06±0.02	
77	52%	-1.03±0.01	0.13±0.02			

Table 4: Results of the fit on $100\,\mathrm{pb}^{-1}$ of data ($2000-2001$ statistics) for different parametrizations of $|A|^2$ and for a total of bins $N_{bin}^{eff}=80$ corresponding to linear dimensions of bins equal to $\Delta X=\Delta Y=0.17$.

7.2 Results of fit on whole statistics

To fit the Dalitz plot distribution, the efficiency has been estimated using a sample of 18.7 millions of events from the new MonteCarlo production. In this sample the problem of fake accidental clusters was resolved using run by run the correction factors [14]. Among these events $\sim 5\%$ are Initial State Radiation (ISR), in which a photon is emitted by the incoming electron or positron. No discrepancy with the previous measurements is observed when fitting with standard parametrization, see eq: (28). With the increased statistics, both data and MC, the theoretical model seems not to fit adequately the data: we found values of χ^2 probability very low, for each *ndf*. Consequently we have expanded the decay amplitude about the center of the Dalitz plot adding the cubic terms:

$$|A(X,Y)|^2 \simeq 1 + aY + bY^2 + cX + dX^2 + eXY + fY^3 + gX^3 + hX^2Y + lXY^2. \tag{35}$$

and we have used this theoretical function to fit the Dalitz plot distribution.
As we expected, for each *ndf* the values of χ^2 probability improve. Moreover we are sensitive to the cubic slope in Y, never measured before; all the other cubic terms different from f are consistent with zero.
The behaviour of the parameter values is shown in fig 20. Again the parameters' values catch up a plateau region, characterized by $N_{bin}^{eff} \in [54, 202]$[8], in which they are almost binning independent.
The final fit results are reported in table 5, in corrispondence of $N_{bin}^{eff}=154$, where we found the better χ^2 probability, and for different parametrizations of $|A|^2$.
Looking at values of χ^2 probability, it is evident that is necessary to fit including both d and f parame-

ndf	P_{χ^2}	a	b	c	d	e	f
147	73%	-1.090±0.005	0.124±0.006	0.002±0.003	0.057±0.006	-0.006±0.007	0.14±0.01
149	74%	-1.090±0.005	0.124±0.006		0.057±0.006		0.14±0.01
150	$<10^{-8}$	-1.069±0.005	0.104±0.005				0.13±0.01
150	$<10^{-10}$	-1.041±0.003	0.145±0.006		0.050±0.006		
151	$<10^{-8}$	-1.026±0.003	0.125±0.006				

Table 5: Results of the fit on full data sample ($450\,\mathrm{pb}^{-1}$) for different parametrizations of $|A|^2$ and for a total of bins $N_{bin}^{eff}=154$ corresponding to linear dimensions of bins equal to $\Delta X=\Delta Y=0.13$.

ters. We clearly observe a quadratic slope in X and a cubic slope in Y different from zero. As expected from the C-invarance in the $\eta\to\pi^+\pi^-\pi^0$ decay the parameters c and e are consistent with zero, moreover can be removed from the fit without affecting the other parameters. In any case a good stability of the

[8]The region $N_{bin}^{eff}\in[54,202]$ corresponds to linear dimensions of bins changing from $\Delta X=\Delta Y=0.20$ to $\Delta X=\Delta Y=0.11$.

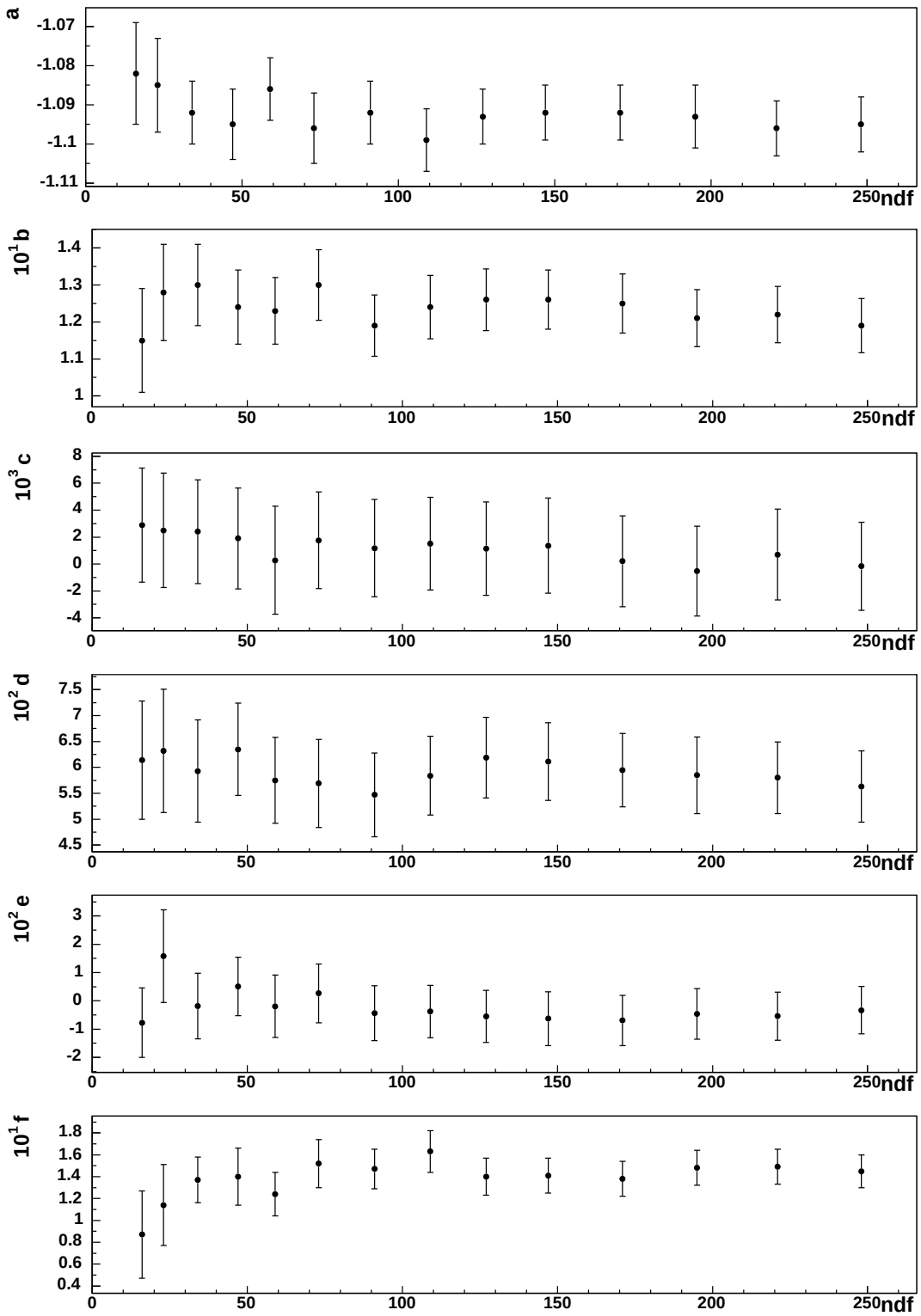

Figure 20: Results of the Dalitz-plot fit on full data sample ($450\,\mathrm{pb}^{-1}$) for different *ndf*. The results refer to a parametrization for the decay amplitude $|A(X,Y)|^2 \simeq 1 + aY + bY^2 + cX + dX^2 + eXY + fY^3$.

parameter values is observed.

Fig.21 shows a comparison between the efficiency corrected data and the fitted function as a function of the bin number, while in fig.22 as a function of the Dalitz plot variables..

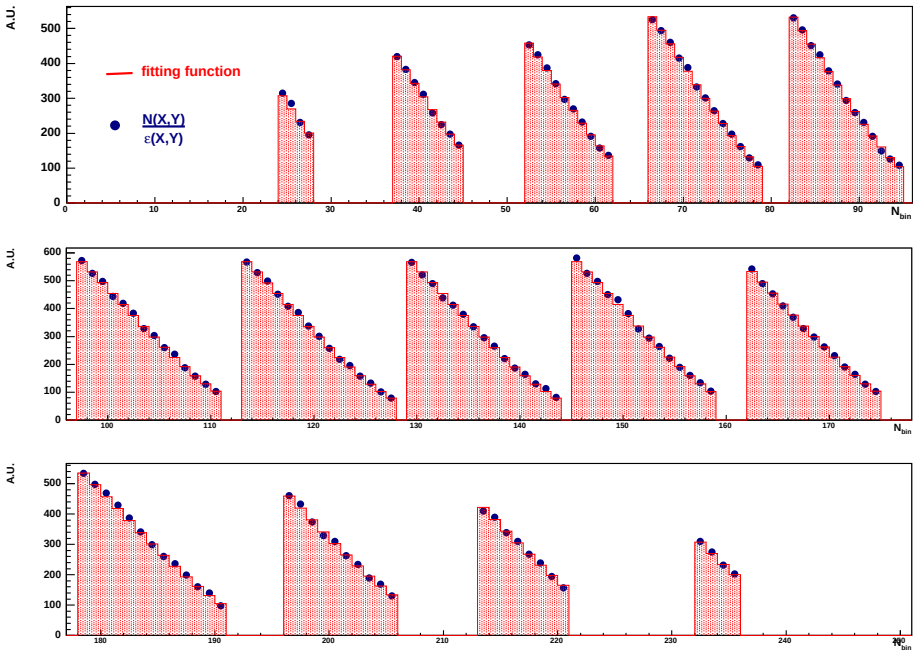

Figure 21: In correspondence of $N_{bin}^{eff} = 154$ a comparison between data and fitted function, $|A(X,Y)|^2 \simeq 1 + aY + bY^2 + cX + dX^2 + eXY + fY^3$, as a function of the bin number. The observed structure corresponds to Y distributions corresponding to slices in X. Blue points are data and the histogram is the function.

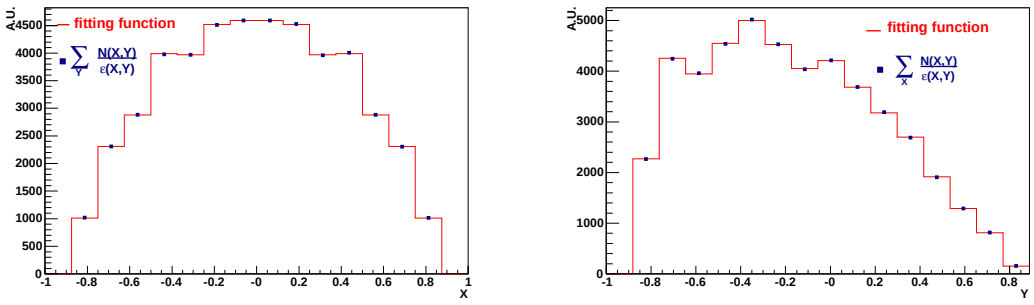

Figure 22: In correspondence of $N_{bin}^{eff} = 154$ a comparison between data and fitted function, $|A(X,Y)|^2 \simeq 1 + aY + bY^2 + cX + dX^2 + eXY + fY^3$, as a function of Dalitz plot variables. Left: X variable. Right: Y variable. Blue points are data and the histogram is the function.

7.3 Check on cubic term 'f'

We have performed some checks to investigate if the sensitivity to the cubic slope in Y on data is a possible effect of efficiency.
Neglecting resolution effects (cfr. fig.12) the fitted function is actually the following:

$$\frac{1}{\varepsilon^{MC}(X,Y)}\frac{dN(X,Y)}{dXdY}_{fit} = \frac{\varepsilon^{REAL}(X,Y)}{\varepsilon^{MC}(X,Y)} \cdot |A(X,Y)|^2 \tag{36}$$

If we assume the cubic term is actually a fake induced by our fitting procedure, the true expansion for $|A(X,Y)|^2$ is:

$$|A(X,Y)|^2 \simeq 1 + aY + bY^2 + dX^2. \tag{37}$$

in which we have neglected the cubic dependency in Y and the odd powers[9] of X.
Now, from the fit we obtain:

$$\frac{1}{\varepsilon^{MC}(X,Y)}\frac{dN(X,Y)}{dXdY}_{fit} \simeq 1 + a'Y + b'Y^2 + d'X^2 + f'Y^3 \tag{38}$$

we can thus define:

$$R(X,Y) \equiv \frac{\varepsilon^{REAL}(X,Y)}{\varepsilon^{MC}(X,Y)} = \frac{1 + a'Y + b'Y^2 + d'X^2 + f'Y^3}{1 + aY + bY^2 + dX^2}. \tag{39}$$

The ratio of the "real" efficiency to the MC one is of course a function of the Dalitz variables X and Y, which in case of perfect MC description should be just a costant equal to 1. We can assume that this function may be expanded itself in powers of X and Y around 1, and we have considered two different cases:

1. $R(X,Y) = 1 + \alpha Y + \beta X^2$.
   From the eq.39, equating the coefficients of the same order up to third order one has this equation system:

$$\begin{cases} a' = a + \alpha; \\ b' = b + a\alpha; \\ d' = d + \beta; \\ f' = \alpha b; \\ \beta a + \alpha d = 0. \end{cases} \tag{40}$$

   Resolving the system in the resonable hypothesys $\alpha < a$, (since we know that a is of order 1) we found:

$$\alpha = 0.3, \qquad \beta = 0.01. \tag{41}$$

   Using these values to reweight the efficiency on MonteCarlo we can compare if the data - MC agreement is improved by this efficiency correction.
   Fig.23 shows the data MonteCarlo discrepancy bin by bin normalized, with efficiency weighed and no. The disagreement observed tells us that the cubic term cannot be accounted for an efficiency correction of the type discussed above.

[9] As seen, cfr. tab.5, the odd power of X are null.

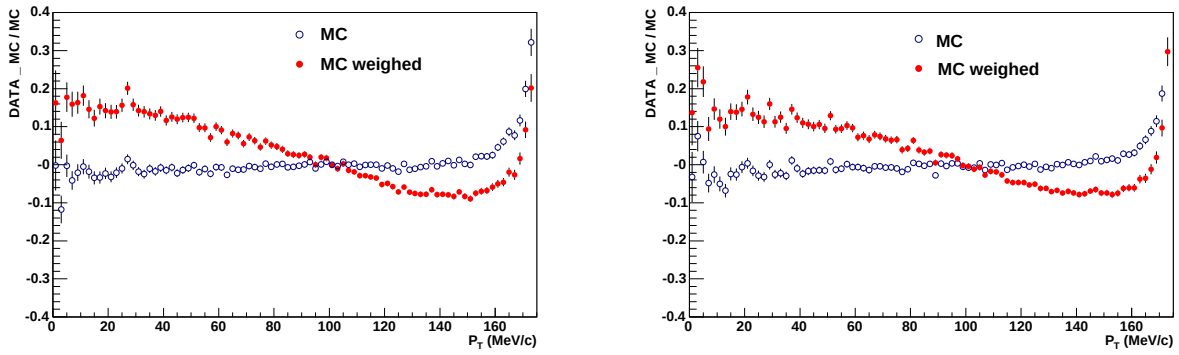

Figure 23: Data vs. MonteCarlo discrepancy bin by bin normalized as function of P_T. With full circles (open circles) efficiency weighed using parameters from eq. 41 (not weighed). Left: π^+ tracks. Right: π^- tracks.

2. $R(X,Y) = 1 + \gamma Y^2$.

   In the efficiency we assume to neglect the linear dependency from Y. As described above we resolve the equation system:

$$\begin{cases} a' = a; \\ b' = b + \gamma; \\ d' = d; \\ f' = \gamma a; \end{cases} \tag{42}$$

   From the fit we obtain for f' and a' respectively a positive and negative value, consequently γ can only assume negative values. We reweight the efficiency using the found value $\gamma = -0.14$. Again, the comparison between MonteCarlo weighed and unweighed, see fig. 24, confirm the our sensitivity to the cubic slope in Y on data.

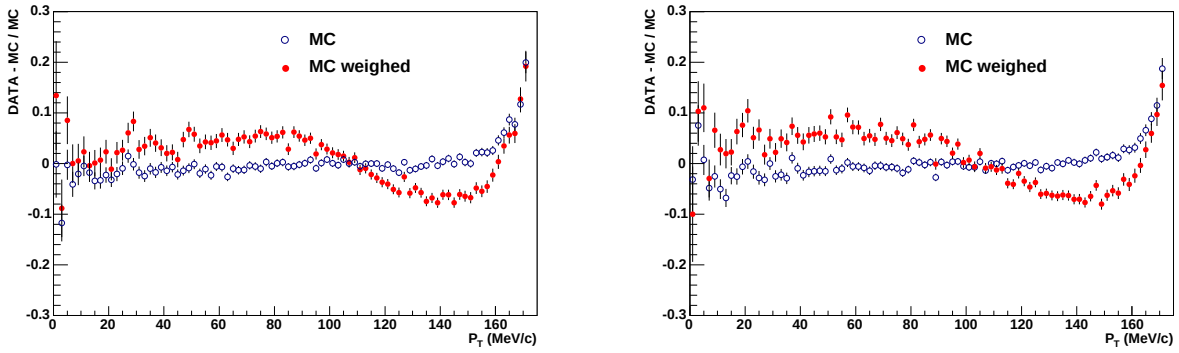

Figure 24: Data vs. MonteCarlo discrepancy bin by bin normalized as function of P_T. With full circles (open circles) efficiency weighed using parameter γ (not weighed). Left: π^+ tracks. Right: π^- tracks.

8 Systematic uncertainties

We have grouped the sources of sistematics on the parameter estimations in:

- resolution and binning
- efficiency evaluation
- background contamination
- effect of EVCL procedure
- stability with respect to data taking conditions

Finally the possible effects of the presence of radiated photons, i.e., radiative corrections, have been considered.
We measured the sistematics in each of these cases and the final results are summarized in table 10.

8.1 Resolution and binning

The $\eta \to \pi^+\pi^-\pi^0$ events selected as described in the previous section are used to study the energy response and resolution of the calorimeter. We therefore have defined:

$$\frac{\Delta E}{E} = \frac{E^{\gamma}_{cl,i} - E^{\gamma}_{true,i}}{E^{\gamma}_{true,i}} \tag{43}$$

where for i^{th} photon, E^{γ}_{true} is the energy in the output of kinematic fit and E^{γ}_{cl} is the energy measured by calorimeter and we have analyzed its distribution as function of E^{γ}_{true}. In particular, we have analysed the distribution of $\frac{\Delta E}{E}$ as function of E^{γ}_{true} dividing the spectrum in bins of 20 MeV. The mean value and the sigma obtained from a gaussian fit are plotted in fig.25 both for data and MonteCarlo. The depenence of the mean value of $\frac{\Delta E}{E}$ on E^{γ}_{true} is weak for both data and MonteCarlo. In data, the photon energy tends to be slightly overestimated, while in MonteCarlo, the photon energy tends to be slightly underestimated; in either case, a drop in response of about 1.5% is observed. This miscalibration decrease to increasing of the energy. The jitters in the distribution of $< \frac{\Delta E}{E} >$ are essentially due to the shape of the photon energy spectrum.
Indeed, since the resolution function is almost symmetric around zero, we expect that in the region where the number of events is increasing as function of E_γ, we get an average correction $\Delta E > 0$, while the opposite applies to region where $N(E_\gamma)$ is decreasing.
This is just related to the fact that the fraction of events in a bin i for which energy has been underestimated (overestimated) is roughly proportional to the number of events in bin $i+1$ $(i-1)$.
A reasonable agreement is observed on resolution, see also fig.26 in which the RMS in bins of E^{γ}_{true} is plotted. For this reason no attempt to fold the theoretical function with a resolution or smearing matrix has been done, moreover the linear dimensions of bin chosen to give the final evaluation for the slope parameters ($\Delta X = \Delta Y = 0.13$) are much larger than the X and Y resolutions ($\delta X = 0.020, \delta Y = 0.019$).

The systematic effect associated to this choice has been evaluated considering for each of the parameter values the maximum and minimum spread in the plateau region (cfr. fig.20) characterized from $N^{eff}_{bin} \in [54, 202]$. A summary of the results is shown in tab.6.

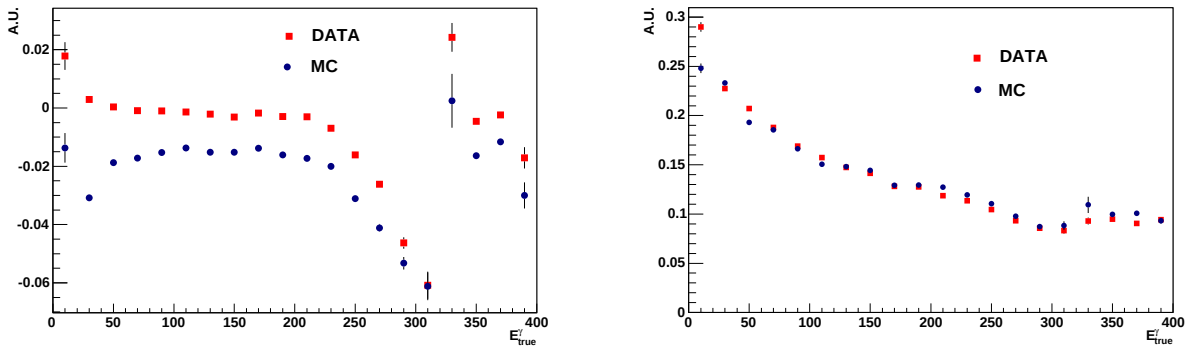

Figure 25: Left: distribution of the mean of the gaussian fit to $\frac{\Delta E}{E}$ as a function of E^{γ}_{true}. Right: distribution of the sigma of the gaussian fit to $\frac{\Delta E}{E}$ as a function of E^{γ}_{true}

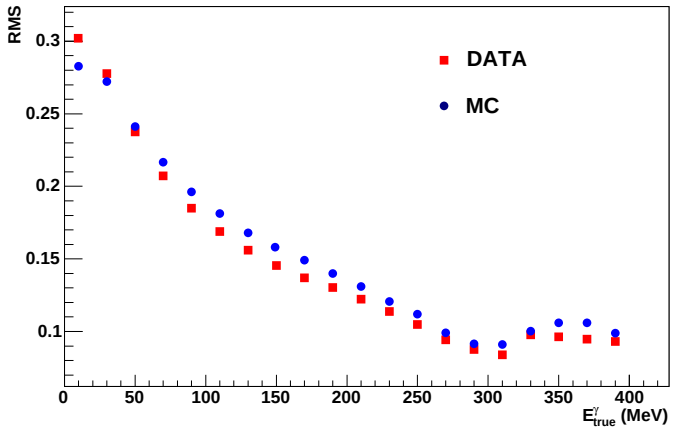

Figure 26: Distribution of the rms in bins of E^{γ}_{true}.

a	b	c	d	e	f
-0.008 +0.006	-0.006 +0.006	-0.001 +0.0	-0.007 +0.001	-0.002 +0.008	-0.02 +0.02
-0.008 +0.006	-0.006 +0.006		-0.007 +0.001		-0.02 +0.02

Table 6: For each of the fit parameters the maximum and minimum spread in the region $N^{eff}_{bin} \in [54, 202]$ or $\Delta X = \Delta Y \in [0.20, 0.11]$ is reported.

8.2 Efficiency evaluation

Since only the shape of the efficiency is relevant for this analysis a reliability check of the MonteCarlo simulation in reproducing the profile of the efficiency has been performed. Anyway, as stated before, the agreement between the observed and the expected overall number of events is within 1.2% (and within errors).

Figs. 28 and 29 show a data vs.MonteCarlo comparison of P_T, P_Z, $\cos\theta$ distributions for tracks, minimum P_T and minimum P_Z among the two charged pions and E_γ for photons. Note that we have used the shift ~ 500 KeV, associated to the different value of the η mass in the MonteCarlo simulation respect to the data (cfr. fig.9), to correct the MonteCarlo P_T distributions.

All the variables used in the comparisons are evaluated in the η rest frame. Some discrepancies in the tails of P_T and P_Z distributions are observed. Cutting on the sidebands of these distributions no significant change in the parameter values has been observed. For the same variables a data MonteCarlo ratio has been evaluated, see figs. 30,31and 32. It is evident a slight slope in P_Z distributions. This slope has been used in correcting the MonteCarlo efficiency, resulting in a negligible effect on the final results.

We use as an estimate of the systematic error the observed discrepancy: $\Delta\epsilon = 0.03\%$.

A correction to low energy photon efficiency is applied weighting the MonteCarlo events. For the photon efficiency we have used a Fermi-Dirac function obtained fitting the photon energy Data-MC discrepancy, see fig.32. For X and Y variables the ratio between the efficiency weighed and no is shown in fig.27. There is an effect at level of per mill but this is negligible for the parameters evaluation.

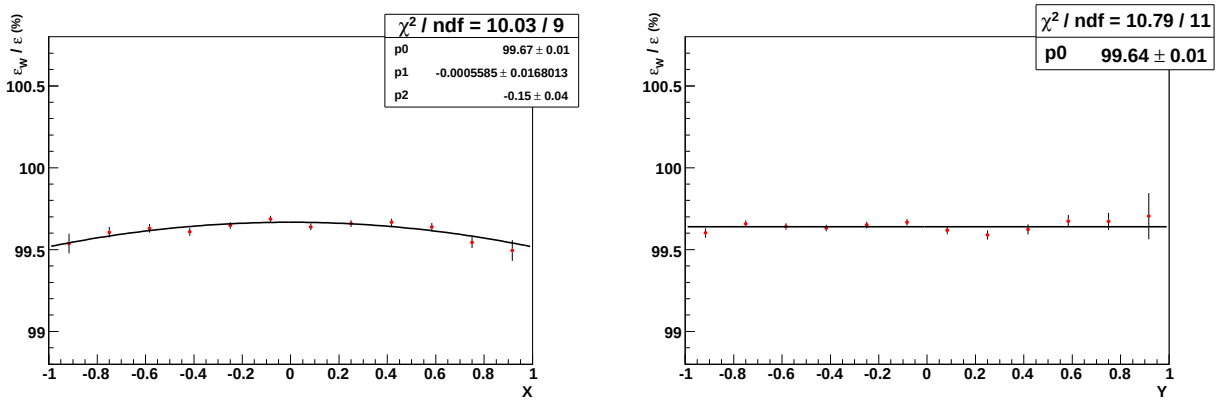

Figure 27: Ratio between weighed and not weighed efficiencies as function of X (Left) and Y (Right). The errors take into account the correlations between the efficiencies.

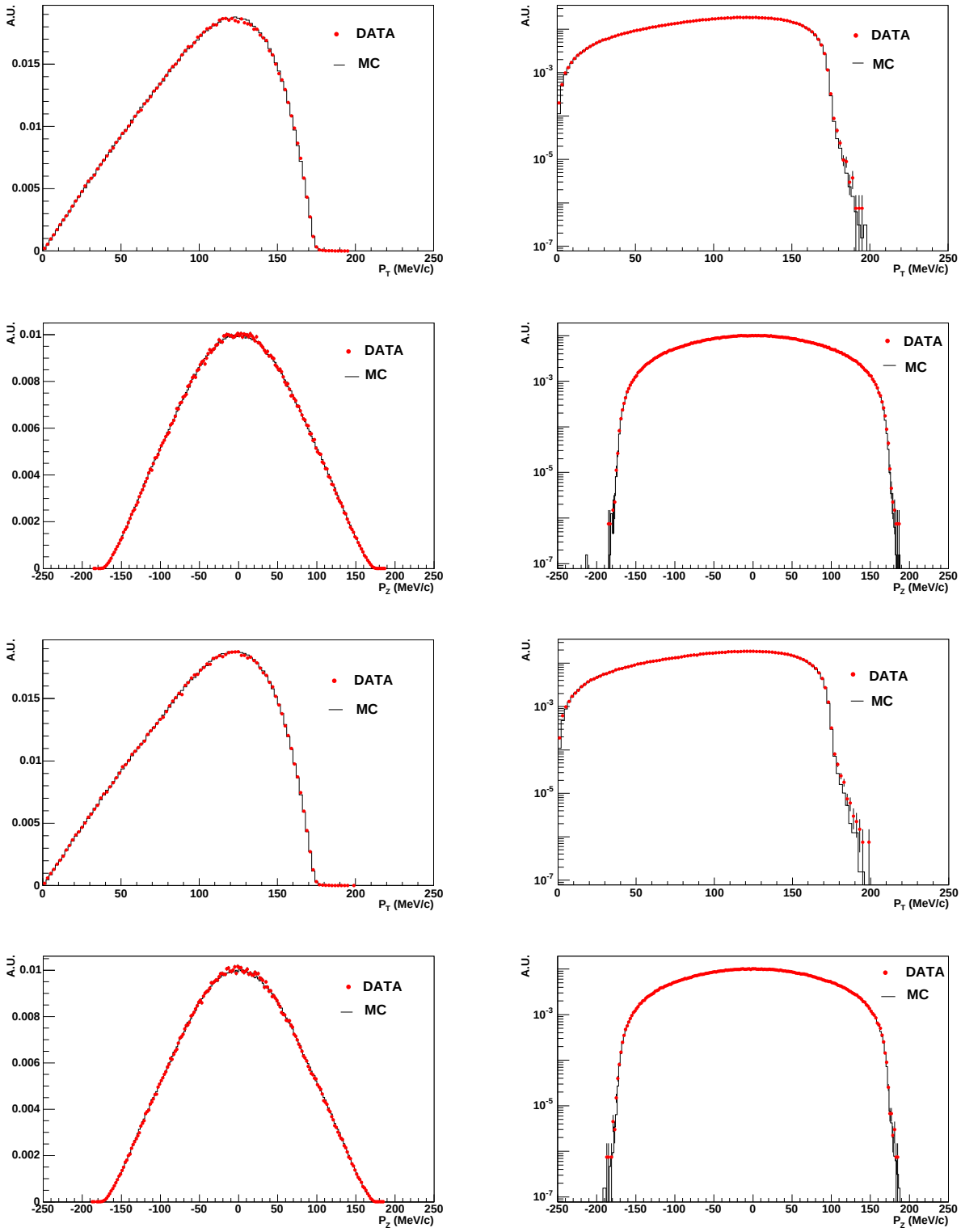

Figure 28: Data vs MonteCarlo comparisons. From top to bottom: P_T, P_Z for $\pi^+$and P_T, P_Z for π^-. Left: linear scale. Right: log scale.

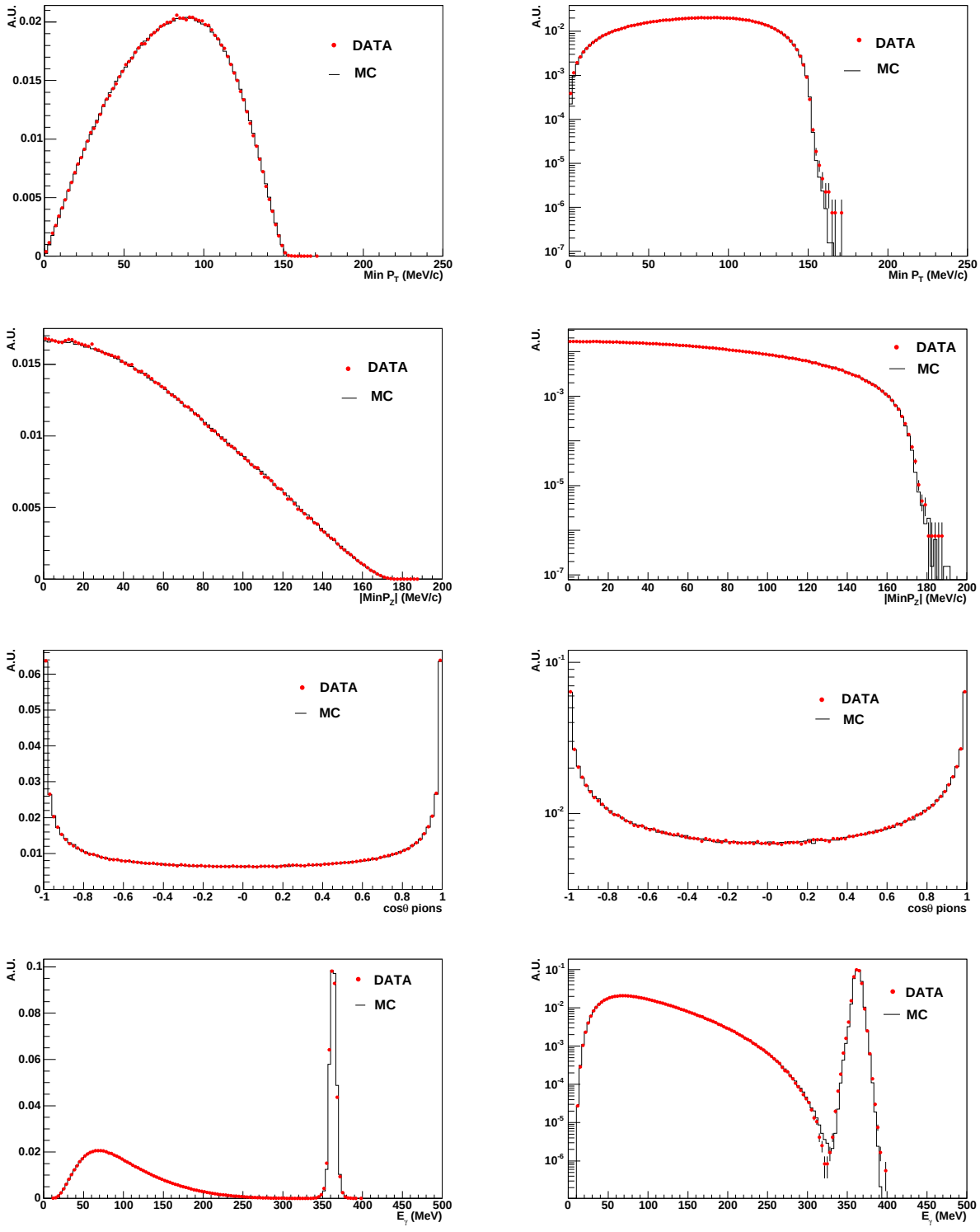

Figure 29: Data vs MonteCarlo comparisons. From top to bottom: minimum P_T and P_Z, $\cos\theta$ between pion tracks and E_γ for photons. Left: linear scale. Right: log scale.

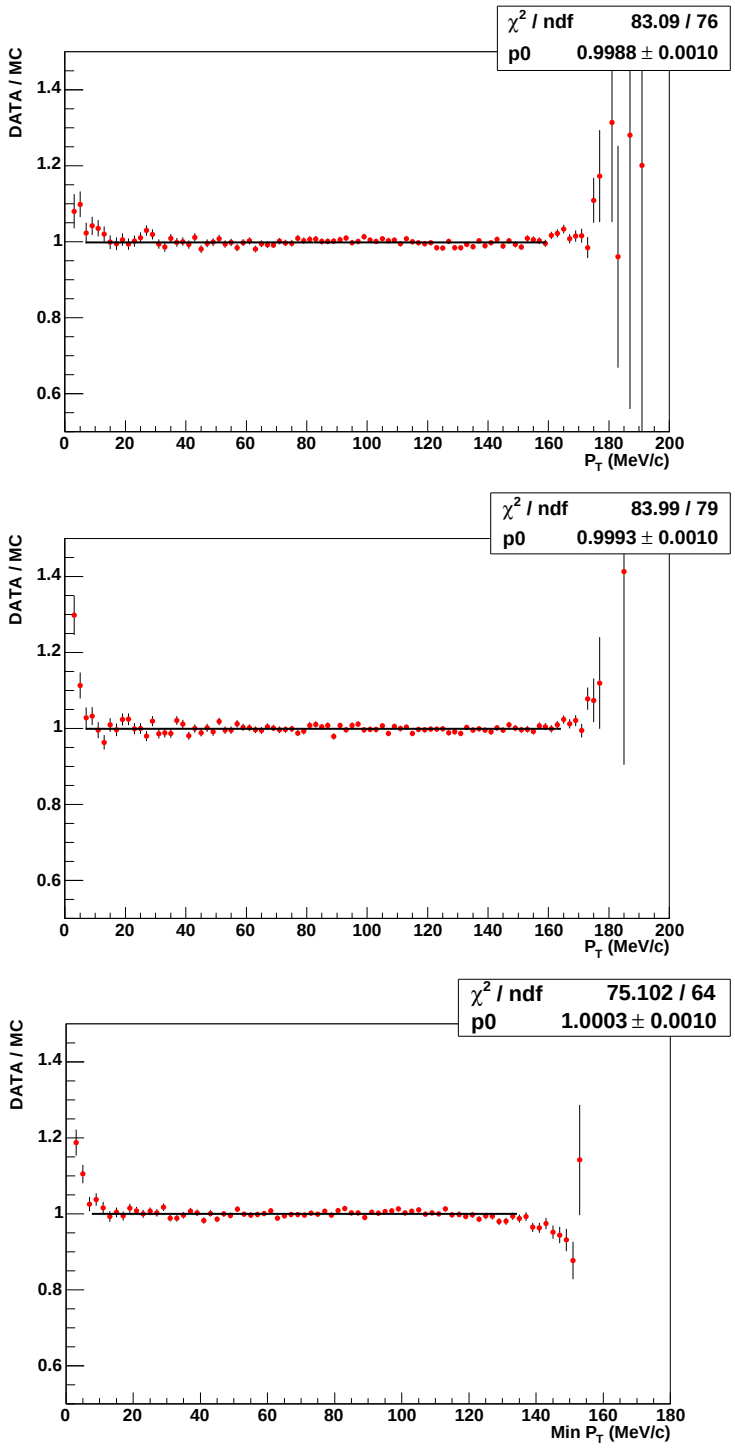

Figure 30: Bin by bin normalized Data/MC ratio for previous plots. The discrepancies which appear in some (less populated) regions have been accounted for in the systematic evaluation. The MonteCarlo histograms are normalized to the same number of events of the data sample. From top to bottom: P_T, for $\pi^+$and π^-, minimum P_T.

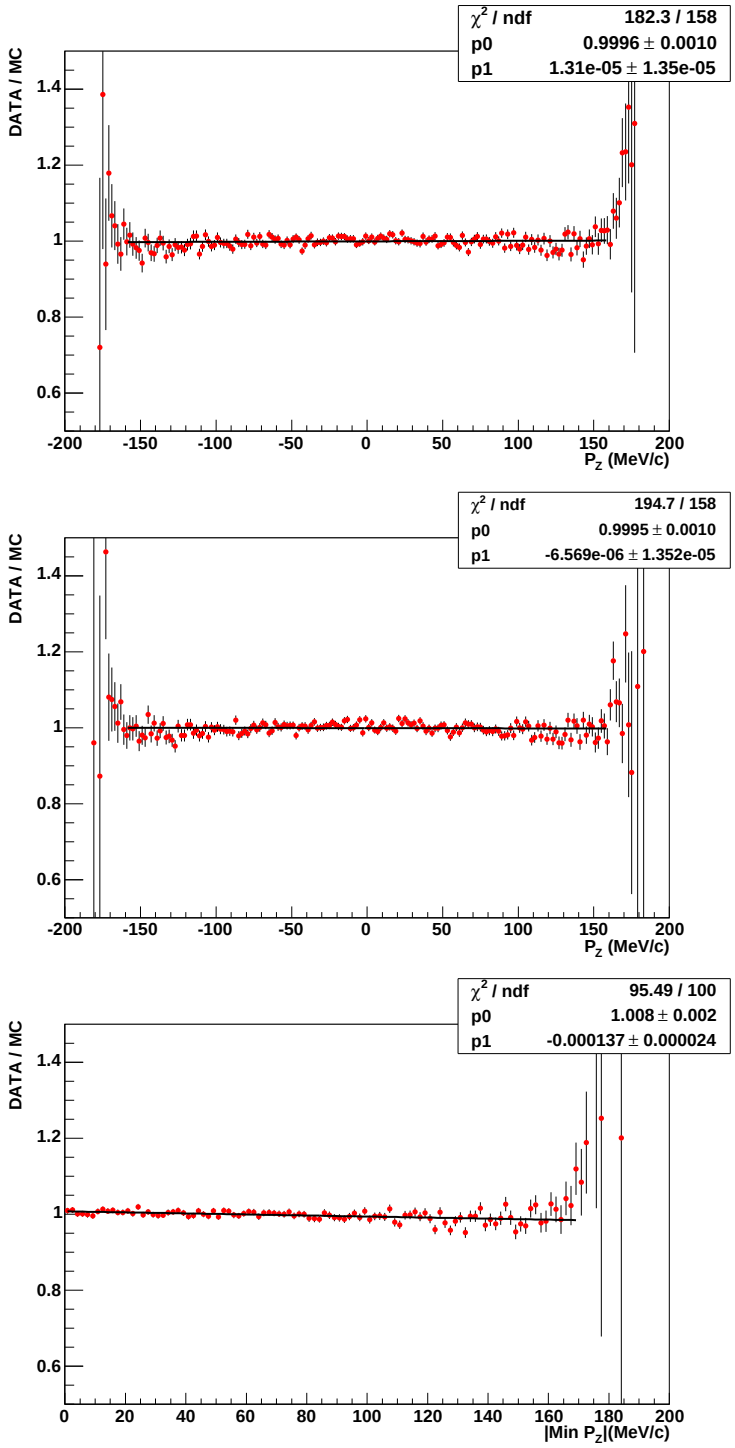

Figure 31: Bin by bin normalized Data/MC ratio for previous plots. The discrepancies which appear in some (less populated) regions have been accounted for in the systematic evaluation. The MonteCarlo histograms are normalized to the same number of events of the data sample. From top to bottom: P_Z for $\pi^+$and π^-, | minimum P_Z|.

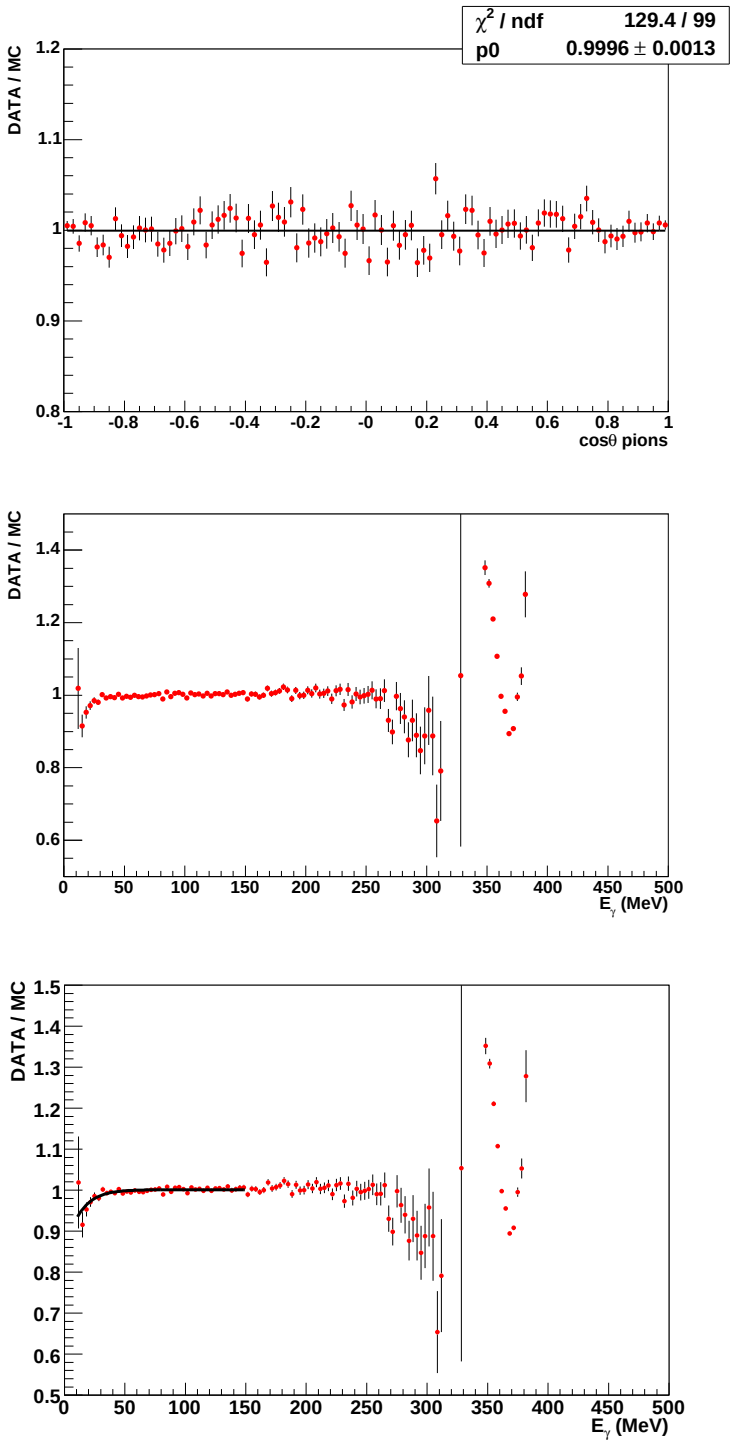

Figure 32: Bin by bin normalized Data/MC ratio for previous plots. The discrepancies which appear in some (less populated) regions have been accounted for in the systematic evaluation. The MonteCarlo histograms are normalized to the same number of events in the data sample. From top to bottom: $\cos\theta$ between pion tracks, E_γ for photons and E_γ for photons with the fit to the Fermi-Dirac function superimposed.

8.3 Background contamination

In order to evaluate the systematic error due to background evaluation we have used the official MonteCarlo "ALL PHYS" production. The data-MonteCarlo comparison for the Y variable (see fig.33) evidences the presence of background. In particular, the background-signal ratio estimated by MonteCarlo is $\sim 0.3\%$.

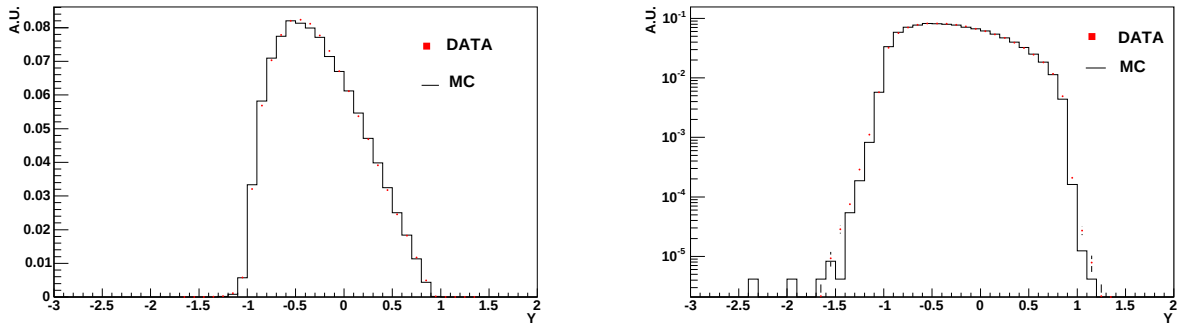

Figure 33: Data vs. MonteCarlo comparison for the Y variable. Left: linear scale. Right: log scale. The MonteCarlo histograms are normalized to the same number of events of the data sample.

The main source of backgrounds considered are:

1. $\phi \to \eta\gamma$ with $\eta \to \pi^+\pi^-\pi^0$ and $\pi^0 \to e^+e^-\gamma$;
2. $\phi \to \omega\pi^0$ with $\omega \to \pi^+\pi^-\pi^0$;

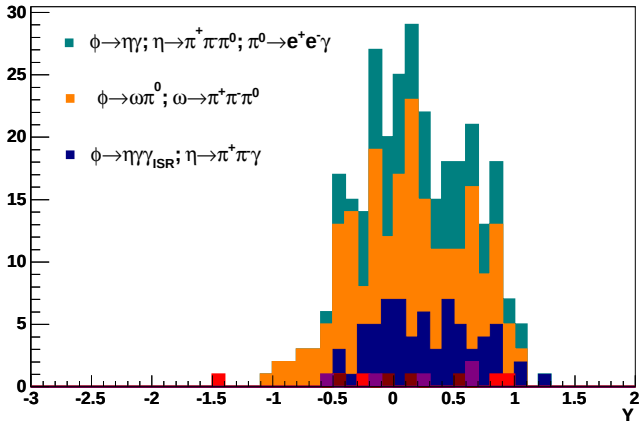

Figure 34: The different contributions to the background evaluation.

Fig.34 shows the estimated amount of these background at the final stage of this analysis. Special care has been devoted in understanding the dependence of background on the cut value for the variable $M_{\gamma\gamma}$[10]

[10] $M_{\gamma\gamma}$ is the invariant mass of the two softest photons in $\pi^+\pi^-\gamma\gamma\gamma$ events.

where significant discrepancies in the tails are observed between data and MonteCarlo (see fig.3). The different amounts of background (estimated from MonteCarlo) obtained changing the values of the cut are reported in tab.7.

$M_{\gamma\gamma}(\mathrm{MeV}/c^2)$	$\frac{B}{S}(\%)$
no cut	0.7
$\in [80, 190]$	0.4
$\in [90, 180]$	0.4
$\in [100, 170]$	0.3
$\in [110, 160]$	0.3
$\in [115, 155]$	0.2
$\in [120, 150]$	0.2

Table 7: For different cuts applied on $M_{\gamma\gamma}$ the related background.

In particular, $\frac{B}{S}$ ratio after the cut $M_{\gamma\gamma} \in [110, 160]$ improves of at least a factor 2, and the background in the region $Y < -1$ is totally rejected, see fig.35. Therefore we apply this cut to give the final fit results.

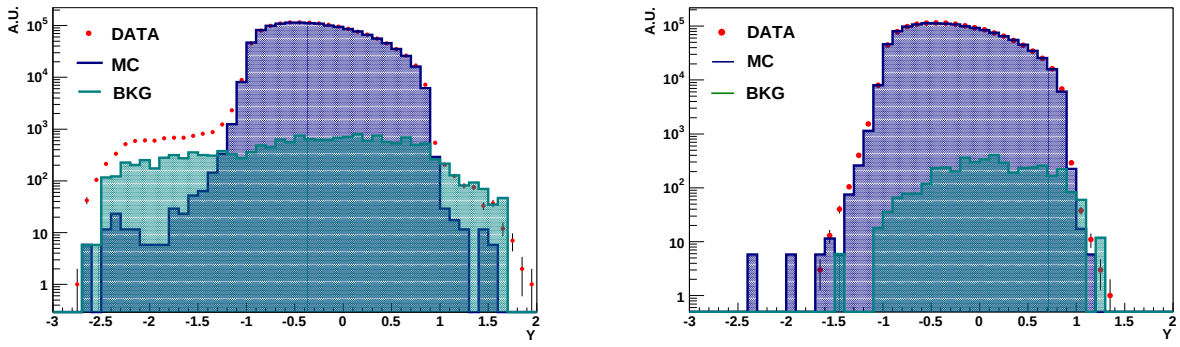

Figure 35: Data-MonteCarlo comparison for the Y distribution. Blue is the MC signal, red dots are the data and green is background. Left: before the cut $M_{\gamma\gamma} \in [110, 160]$. Right: after the cut $M_{\gamma\gamma} \in [110, 160]$.

We have estimated the Dalitz-plot parameters changing the values of the cut on $M_{\gamma\gamma}$, a summary of the results obtained is shown in tab.8.

Finally, for each parameter we quote as a systematic error due to the background evaluation the maximum and minimum spread between the different fits, see tab.9

	P_{χ^2}	a	b	d	f
(1)	82%	-1.084±0.005	0.116±0.006	0.050±0.006	0.14±0.01
(2)	82%	-1.086±0.005	0.117±0.006	0.052±0.006	0.14±0.01
(3)	75%	-1.087±0.005	0.118±0.006	0.053±0.006	0.14±0.01
(4)	**74%**	**-1.090±0.005**	**0.124±0.006**	**0.057±0.006**	**0.14±0.01**
(5)	71%	-1.091±0.005	0.128±0.006	0.060±0.006	0.14±0.01
(6)	58%	-1.089±0.006	0.130±0.006	0.064±0.006	0.13±0.01

Table 8: Results of the Dalitz plot fit after subtracting the background and for different cut on $M_{\gamma\gamma}$: (1) $M_{\gamma\gamma} \in [80, 190]$, (2) $M_{\gamma\gamma} \in [90, 180]$ (3) $M_{\gamma\gamma} \in [100, 170]$, (4) $M_{\gamma\gamma} \in [110, 160]$, (5) $M_{\gamma\gamma} \in [115, 155]$, (6) $M_{\gamma\gamma} \in [120, 150]$. The final fit results are in correspondence of (4).

a	b	d	f
-0.001 +0.006	-0.008 +0.006	-0.007 +0.007	-0.01

Table 9: For each of the fit parameters the systematic error due to the background subtraction is reported.

8.4 Effect of EVCL procedure

We have evaluated the systematic uncertainty induced by the EVCL procedure using a data sample of $23\,\mathrm{pb}^{-1}$ (Minimum Bias sample) selected as described in [16].
No bias in reproducing the shape of efficiency is introduced by EVCL procedure. The Dalitz plot distribution has been fitted both without requiring the EVCL procedure (i.e. using the full Minimum Bias sample) and requiring the EVCL tag. For each parameter, we quote as systematic uncertainty the difference among the two obtained values: this is due to the fact that since the two samples are 98.5% correlated, any difference between the two fits is statistically significant.

	a	b	d	f
Minimum Bias AND EVCL	-1.050 ± 0.024	0.153 ± 0.027	0.057 ± 0.026	0.080 ± 0.054
Only Minimum Bias	-1.067 ± 0.024	0.158 ± 0.027	0.045 ± 0.025	0.090 ± 0.053

8.5 Time stability

We have checked the stability of the parameter values with respect to the data taking conditions.
We have checked both large scale uniformity and small scale uniformity. On a *large scale* we have split the full data sample in 9 bunches of about $50\,\mathrm{pb}^{-1}$ each and repeated the fit procedure in order to estimate all the parameters. The results, together with the fit to a constant function, are shown in fig. 36.

On a *small scale* the data sample has been split in subsamples of almost equal integrated luminosity, $5\,\mathrm{pb}^{-1}$, and for each of these we have fitted the Dalitz plot distribution. Since we have low statistics in each sample we have fitted using a one dimensional fit procedure (see Appendix A) where we are sensitive only to the linear and quadratic slopes in Y. For both parameters the time dependency is compatible with a costant function, see fig.37.

8.6 Radiative correction

Finally we have studied also the possible effects of the radiative corrections in the final state to the Dalitz plot density. To include the radiative correction in the MonteCarlo simulation we have used a generator $\eta \to \pi^+\pi^-\pi^0\,\gamma$ provided us by C.Gatti.
In fig.38 is shown the distribution of Dalitz plot for the events $\eta \to \pi^+\pi^-\pi^0\,\gamma$.
In this MonteCarlo version we have used the same values for a, b, d parameters as in the standard one. Then we have checked that our fit procedure gives in output the same values for the above parameters with an accuracy comparable with the one shown in fig. 19.
Moreover we have verified that the bin by bin ratio of the two MonteCarlo distributions (see fig.38) can be fitted with a constant with $\chi^2/\mathrm{dof} = 154/153$ corresponding to a χ^2 probability of 46%

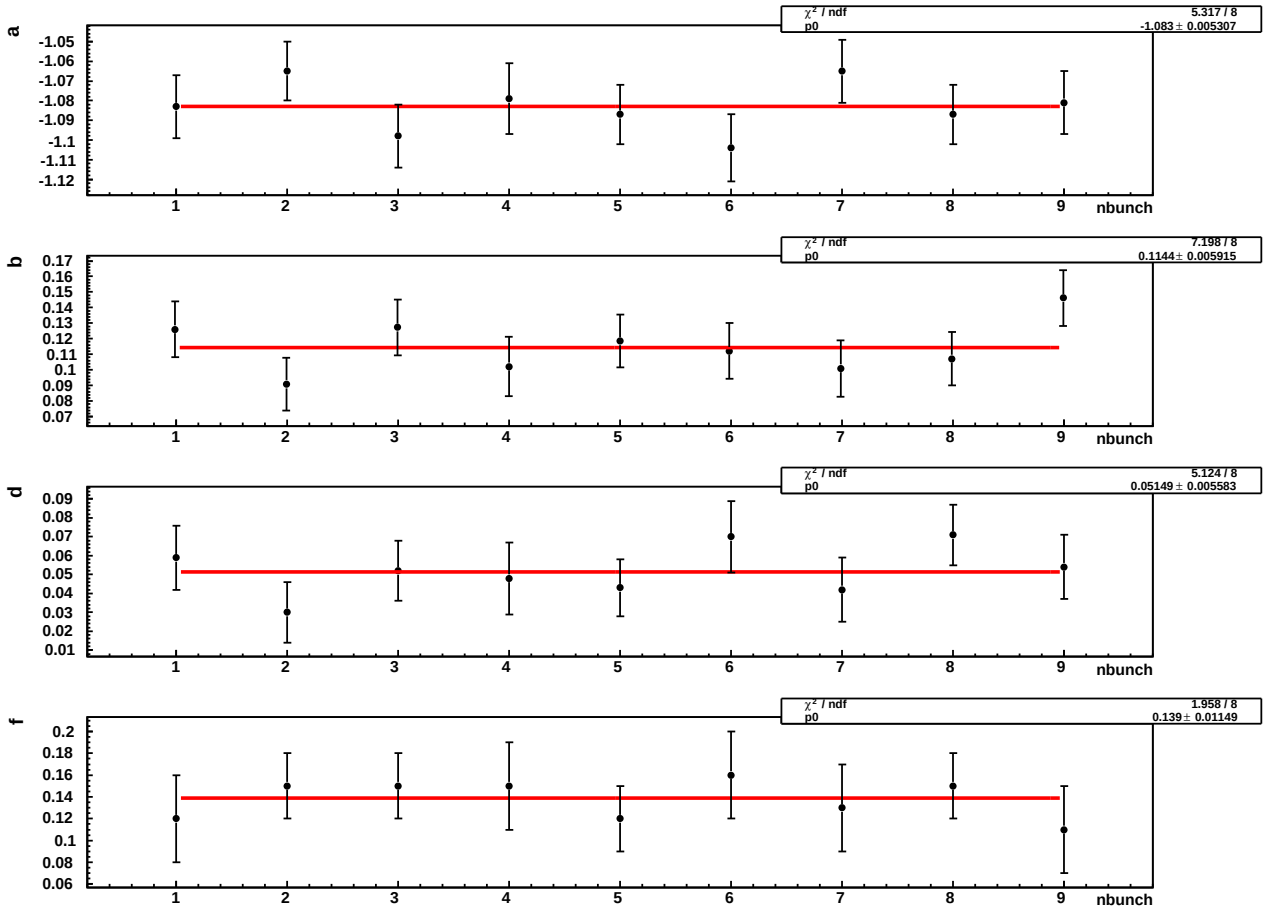

Figure 36: Fit parameters as function of time along data taking. The data sample has been split in subsample having the same integrated luminosity. The results of a fit with costant function is reported.

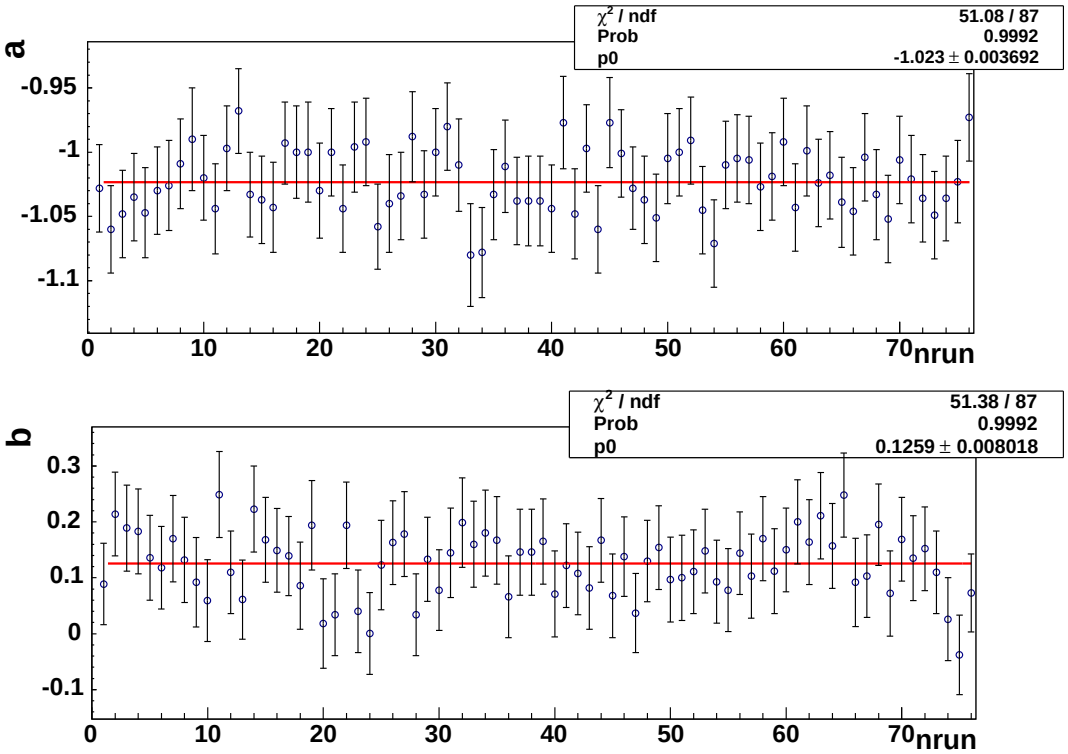

Figure 37: Behaviour of the linear and quadratic slopes in Y as function of the time. The data sample has been split in subsample having the same integrated luminosity. The results of a fit with costant function is reported.

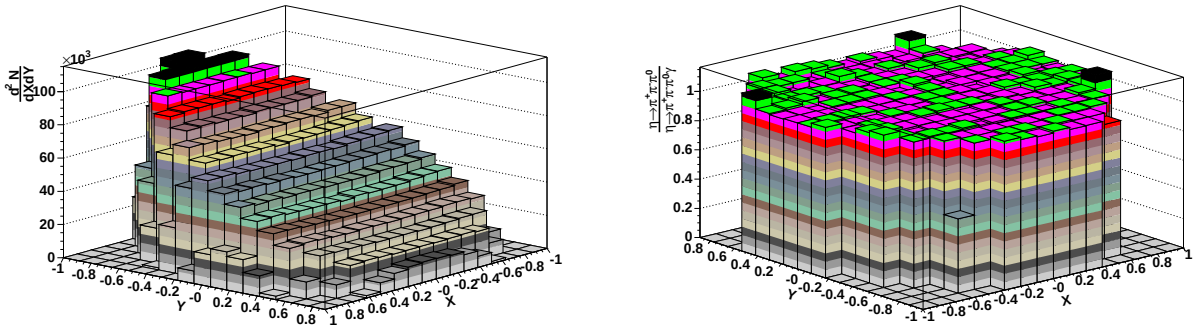

Figure 38: Left: Dalitz plot distribution for events $\eta \to \pi^+\pi^-\pi^0\,\gamma$. The plot contains 10.0 millions of events. Right: Bin by bin ratio of Dalitz distribution of $\eta \to \pi^+\pi^-\pi^0$ and $\eta \to \pi^+\pi^-\pi^0\,\gamma$ events.

For each of the fit parameters a summary of the most relevant systematic errors are reported in tab.10.

Source	Δa	Δb	Δd	Δf
BKG	-0.001 +0.006	-0.008 +0.006	-0.007 +0.007	-0.01
BIN	-0.008 +0.006	-0.006 +0.006	-0.007 +0.001	-0.02 +0.02
EVCL	-0.017	0.005	-0.012	0.01

Table 10: For each of the fit parameters a summary of the systematic errors.

9 Asymmetries

While the polynomial fit of the Dalitz plot density gives valuable information on the matrix element, some integrated asymmetries are very sensitive in assessing the possible contributions to C violation in amplitudes with fixed ΔI. In particular left-right asymmetry (which is of course strongly related to the c parameter in our fit) tests C violation with no specific ΔI constraint; quadrant asymmetry tests C violation in $\Delta I = 2$ and sextant asymmetries tests C violation in $\Delta I = 1$. The present experimental results date back to the 70's and are reported by PDG as in table 11. We have analyzed 4 times the total

Left-Right	Quadrant	Sextant
$(0.09 \pm 0.17) \times 10^{-2}$	$(-0.17 \pm 0.17) \times 10^{-2}$	$(0.18 \pm 0.16) \times 10^{-2}$

Table 11: Dalitz plot asymmetries from PDG.

statistics which enters the PDG averages, and we can thus improve these results. The approach we use for this measurement is the following: we obtain from MC the efficiency for each region of the Dalitz plot just as the number of events reconstructed in that region divided by the number of events generated in that particular region. This definition takes into account the resolution effects as well. We cross check the result by evaluating the asymmetries on Monte Carlo, these turn out to be all compatible with zero. We then evaluate the asymmetry on data by folding the expected MC efficiency. Of course before doing this we subtract from data the expected background Dalitz plot obtained from MC. On MC, for a sample of 5.69×10^6 events we get:

$$\varepsilon_L = (34.91 \pm 0.02)\% \qquad \varepsilon_R = (35.05 \pm 0.02)\%$$
$$\varepsilon_{13} = (35.01 \pm 0.02)\% \qquad \varepsilon_{24} = (34.95 \pm 0.02)\%$$
$$\varepsilon_{135} = (35.00 \pm 0.02)\% \qquad \varepsilon_{246} = (34.96 \pm 0.02)\%$$

The "raw" asymmetries on data are found to be:

$$A_{LR} = (-0.09 \pm 0.09) \times 10^{-2}$$
$$A_Q = (0.02 \pm 0.09) \times 10^{-2}$$
$$A_S = (0.13 \pm 0.09) \times 10^{-2}$$

Correcting for MC efficiencies we get:

$$A_{LR} = (0.09 \pm 0.10(stat.)) \times 10^{-2}$$

$$A_{Q} = (-0.05 \pm 0.10(stat.)) \times 10^{-2}$$

$$A_{S} = (0.08 \pm 0.10(stat.)) \times 10^{-2}$$

In assessing the systematics for the measured asymmetries we have considered all the effects taken into account for the Dalitz plot fit, namely:

- Effect of background (by varying cuts);
- Effect of EVCL (by using Minimum Bias sample);
- DATA/MC efficiency comparison (using the $\phi \to \pi^+\pi^-\pi^0$ control sample)

In particular the tracking efficiency has been evaluated separately for the two charges, since it is evident on MC that there is a small but statistically significant difference in left and right efficiencies, pointing to a slightly different tracking efficiency as a function of p_T for positive and negative pions. We emphasize that, again, since we ask for both tracks being reconstructed, it is not the absolute value of efficiencies which is important for the asymmmetry, but rather its dependence upon the pion momentum. The very good DATA/MC agreement has been already demonstrated for both charges on the signal. We here use an independent control sample of $\phi \to \pi^+\pi^-\pi^0$ events and, as described before (see section 3.2), check the agreement between Data and MC for the efficiencies as a function of momentum the two charges. Results are shown in fig. 39.

The control sample agrees very well with MC within error, and the DATA/MC ratio is well fitted by a constant.

In order to assess the possible systematics connected with the efficiencies we have assumed a "worst case" approach: we have built the maximum and minimum slope compatible within one sigma with the constant appearing in the fits shown in fig. 39. The we have assumed the two charges to behave with the *opposite* slopes. This gives us two possibilities (π^+ with positive slope and π^- with negative slope and vice-versa). We have then reweighted the events according to these two possibilities and used the maximum difference observed in the asymmetries as an estimate of the possible systematic effects due to different DATA/MC efficiencies. Finally we can summarize the systematics connected with the asymmetries as:

Syst. Effect	Left-Right	Quadrant	Sextant
Background	$(-0.2/+0.1) \times 10^{-3}$	$(-0.2/+0.2) \times 10^{-3}$	$(+0.3) \times 10^{-3}$
EVCL	$(-0.5) \times 10^{-3}$	$(-0.3) \times 10^{-3}$	$(+0.7) \times 10^{-3}$
Efficiency	$(-1.3/+0.9) \times 10^{-3}$	$(-0.3/+0.2) \times 10^{-3}$	$(-1.3) \times 10^{-3}$
TOTAL	$(-1.4/+0.9) \times 10^{-3}$	$(-0.5/+0.3) \times 10^{-3}$	$(-1.3/+0.8) \times 10^{-3}$

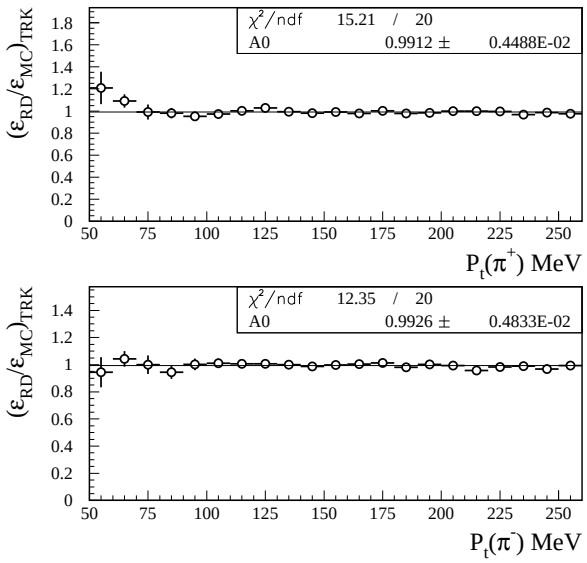

Figure 39: The Data/MC ratio of tracking efficiency for π^+ (up) and π^- (down) as a function of the pion transverse momentum. The error from the fitting constant have been used for systematics evaluation (see text).

We can thus summarize the results for the asymmetries as follows:

$$A_{LR} = (0.09 \pm 0.10(\text{stat.})^{+0.09}_{-0.14}(\text{syst.})) \times 10^{-2}$$

$$A_Q = (-0.05 \pm 0.10(\text{stat.})^{+0.03}_{-0.05}(\text{syst.})) \times 10^{-2}$$

$$A_S = (0.08 \pm 0.10(\text{stat.})^{+0.08}_{-0.13}(\text{syst.})) \times 10^{-2}$$

We can conclude (in agreement with the null value of the c and e parameters in our fit), that we find no evidence for C violation in the $\eta \to \pi^+\pi^-\pi^0$ decay.

10 Conclusions

The results including the statistical uncertainties coming from the fit and the estimate of systematics are:

$$a = -1.090 \pm 0.005(stat)^{+0.008}_{-0.019}(syst) \tag{44}$$

$$b = 0.124 \pm 0.006(stat) \pm 0.010(syst) \tag{45}$$

$$d = 0.057 \pm 0.006(stat)^{+0.007}_{-0.016}(syst) \tag{46}$$

$$f = 0.14 \pm 0.01(stat) \pm 0.02(syst) \tag{47}$$

Note that the systematic error has been obtained adding in quadrature all the contributions in table 10. Tab.12 gives the correlation coefficients between the fitted parameters.

In fig.40 are shown the normalized residuals as function of bin number. The following comments can be

	a	b	d	f
a	1	-0.226	-0.405	-0.795
b		1	0.358	0.261
d			1	0.113
f				1

Table 12: Correlation matrix from the Dalitz-plot fit.

done:

- the fitted value for the quadratic slope in Y is almost one half of the simple Current algebra prediction ($b = a^2/4$) thus calling for important higher order corrections;
- the quadratic term in X is unambiguously found different from zero;
- the same applies for the unexpectedly large cubic term in Y;
- the strong correlations between parameters imply that much care must be taken when integrating the polynomial over the phase space, since error propagation for the result must correctly take correlations into account;
- for the a, b, d parameters, which have not been measured here for the first time, we observe a reasonable agreement with the ones in literature, see fig. 41 especially taking into account that for all previous measurements only statistical errors were considered.

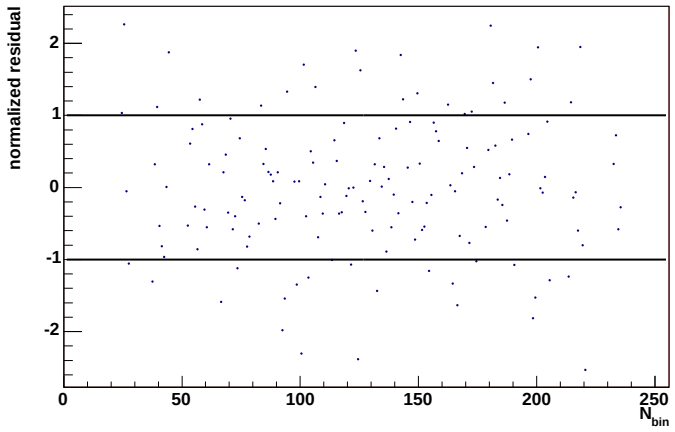

Figure 40: Distribution of the normalized residual. As expected, the residuals fluctuate around to the zero.

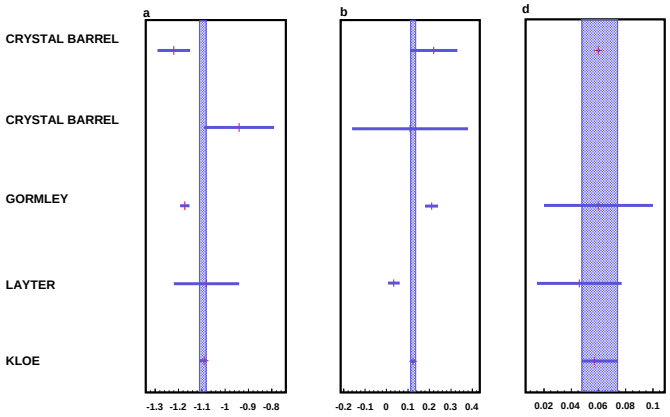

Figure 41: Comparison between the values of the Dalitz plot parameters obtained in the present analysis (solid squares) and in the measurements considered by the PDG [18] (red dots). In the plot the error on the parameters of this analysis has been obtained adding in quadrature the statistical and systematic error while for the other measurements only the statistical error is reported.

11 Acknowledgements

We would like to thank C. Gatti for providing us the MC generator for radiative eta decay.
We say thank you also to the referees Giorgio Capon and Antonella Antonelli, for very interesting discussions and suggestions that helped us to complete this job. Finally, we would like to thank Camilla Di Donato for helping us but especially to have supported us “many times” during this job.

12 Appendix A

In this appendix we show the one dimensional fit procedure.
Let $|A(Y)|^2 \simeq 1+aY+bY^2$ the amplitude of decay in which we have neglected every dependency from X.
In general, the density of points in the Dalitz-plot is proportional to the square of the invariant matrix element for the decay, then one has:

$$|A(Y)|^2 = \frac{\sum_{N_{binx}} \frac{N(X,Y)}{\varepsilon(X,Y)}}{\int_{phase\ space} dx} \tag{48}$$

where

- $N(X,Y)$ are the number of events in the Dalitz-plot,
- $\varepsilon(X,Y)$ is the efficiency as function of Dalitz-plot,

and when summing over X bins we have applied a phase space correction.
Thus, fitting the eq.48 with a polynomial we obtain an estimate of the parameters.
In fig.42 are shown the results of fit with two different parametrization.

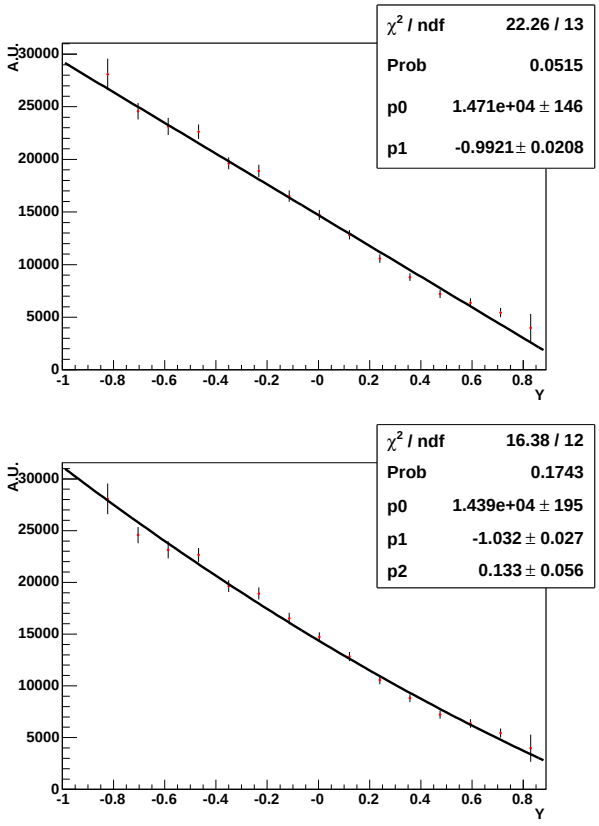

Figure 42: Results of fit to the Dalitz-plot density. Top: $|A(Y)|^2 \simeq N_0(1+aY)$. Bottom: $|A(Y)|^2 \simeq N_0(1+aY+bY^2)$.

References

[1] D.G. Sutherland, Phys.Lett. **23**, 384 (1966)

[2] R. Baur, J. Kambor and D. Wyler Nucl. Phys. **B460**, 127 (1966)

[3] J. Bijnens and J. Gasser, Physica Scripta **T99**, 34 - 44 (2002)

[4] R. Dashen, Phys.Rev. **183**, 1245 (1969).

[5] B. Holstein, Physica Scripta **T99**, 55 - 67, (2002)

[6] J. Gasser and H. Leutwyler, Ann.Phys.(NY) **150** 142, (1984); Nucl.Phys.**B250** 465, (1985).

[7] J. Kambor, C. Wiesendanger and D. Wyler, Nucl.Phys. **B465**, 215 (1996).

[8] J.G. Layter *et al.*, Phys.Rev. **D7**, 2565 (1973).

[9] M. Gormley *et al.*, Phys.Rev **D2**, 501 (1970).

[10] Crystal Barrel Collaboration, Phys.Lett. **B346**, 203 (1995).

[11] Crystal Barrel Collaboration, Phys.Lett. **B417**, 197 (1998).

[12] F. Ambrosino *et al.*, KLOE memo 225 (2000).

[13] M. Adinolfi *et al.*, [KLOE Collaboration] Nucl. Instrum. Meth. **A461**, 344 (2001)

[14] M. Martini, S. Miscetti, KLOE memo 303 (2005).

[15] F. Ambrosino , KLOE note 179 (2002).

[16] C. Di Donato , KLOE memo 306 (2005).

[17] C. Di Donato , KLOE memo 327 (2006).

[18] W. M. Yao *et al.*, J. Phys. G. **33**,1 (2006).

[19] M. Dreucci , "*Phi lineshape*" presented at KLOE workshop, Capri (2003).

[20] S. Giovannella, S. Miscetti , KLOE note 177 (2002).

[21] A. Lay *et al.*, Phys. Lett. **B533**, 196 (2002).